

---

# Electromagnetic probes

Rupa Chatterjee<sup>1</sup>, Lusaka Bhattacharya<sup>2</sup>, and Dinesh K. Srivastava<sup>1</sup>

<sup>1</sup> Variable Energy Cyclotron Centre, 1/AF, Bidhan Nagar, Kolkata 700064, India,  
[rupa@veccal.ernet.in](mailto:rupa@veccal.ernet.in), [dinesh@veccal.ernet.in](mailto:dinesh@veccal.ernet.in)

<sup>2</sup> Saha Institute of Nuclear Physics, 1/AF, Bidhan Nagar, Kolkata 700064, India,  
[lusaka.bhattacharya@saha.ac.in](mailto:lusaka.bhattacharya@saha.ac.in)

**Summary.** We introduce the seminal developments in the theory and experiments of electromagnetic probes for the study of the dynamics of relativistic heavy ion collisions and quark gluon plasma.

## 1 Introduction

Collision of heavy nuclei at relativistic energies is expected to lead to formation of a deconfined state of matter known as Quark-Gluon Plasma (QGP) [1], where quarks and gluons are the effective degrees of freedom rather than nucleons or hadrons [2, 3]. It is now well accepted that a few microseconds after the ‘Big Bang’ the whole universe was in the state of QGP [4].

Several experiments performed at the Super Proton Synchrotron (SPS) at CERN and Relativistic Heavy Ion Collider (RHIC) at Brookhaven National Laboratory, New York, have provided a significant evidence of the formation of this novel state of matter. A giant accelerator known as Large Hadron Collider (LHC) at CERN will be in operation very soon and will provide many new insights about the properties of QGP and the theory of strong interactions.

Heavy ion collisions at relativistic energies produce extremely high temperatures and energy densities within a very small volume. As a result, quarks and gluons (also known as partons) no longer remain confined within the nucleonic volume and create a deconfined state of partons due to multiple scatterings and production of secondaries due to gluon multiplications. The system (or the fireball) may reach a state of local thermal equilibrium. It cools by expansion and below a certain critical temperature ( $T_c \sim 180$  MeV) or energy density, the partons are confined to form hadrons and the system reaches a hadronic state. It may undergo a further expansion and cooling before the freeze-out takes place.

Radiation of photons and dileptons has been proposed as the most promising and efficient tool to characterize the initial state of heavy ion collisions.

Unlike hadrons, which are emitted from the freeze-out surface after undergoing intense re-scatterings, photons come out from each and every phase of the expanding fireball. Being electromagnetic in nature, they interact only weakly and their mean free path is larger than the typical system size ( $\sim 10$  fm). As a result once produced, they do not suffer further interaction with the medium ( $\alpha \ll \alpha_s$ ) and carry undistorted information about the circumstances of their production to the detector [5].

Initially, photons (real as well as virtual), were studied in order to get only the temperature of the plasma. Several other possibilities, e.g., (i) evolution of the system size by intensity interferometry [6], (ii) momentum anisotropy of the initial partons [7] as well as formation time of quark-gluon plasma [8] using elliptic flow of thermal photons, (iii) an accurate check on jet quenching and other aspects of the collision dynamics by photons due to passage of high energy jets through plasma [9] etc. have come to the fore. Of-course dileptons are considered as the most reliable messengers of the medium modification of vector mesons [10].

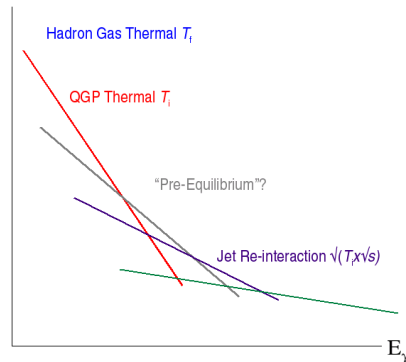


**Fig. 1.** Schematic diagram of different sources of photons and their relative  $p_T$  spectra.

## 2 Sources of photons

In order to proceed, it is useful to identify various sources of photons from relativistic heavy ion collisions. Their production is a result of convolution of the emissions from the entire history of the nuclear collision. Photons are emitted from the pre-equilibrium stage, from QGP phase, from hadronic phase and also from the decay of hadrons produced at the time of freeze-out. An ideal situation would ensue if the contributions from different stages dominate different parts of the  $p_T$  spectrum. A schematic diagram of the different sources of photons and their slopes is shown in Fig. 1. We, thus need rates

and models to study the evolution from different sources. Hydrodynamics, Cascade, Fire-ball, Cascade+Hydrodynamics are the vastly used models for this purpose.

## 2.1 Direct photons

The term ‘direct photons’ stands for the photons which emerge directly from a particle collision. In a heavy ion collision experiment, the detector captures all the emitted photons including those from decay of final state hadrons. The resultant spectrum is the inclusive photon spectrum. However, more than 90% of the photons in this spectrum are from hadron decay. One can subdivide this broad category of ‘direct photons’ into ‘prompt’, pre-equilibrium, ‘thermal’ (from QGP as well as hadronic phase) and ‘jet conversion’ depending on their origin. Before we come to the different sub-categories of direct photons, we start our discussion with decay photons and their subtraction from the inclusive photon spectrum.

## 2.2 Decay Photons

As mentioned earlier, most of the decay photons are from 2- $\gamma$  decay of  $\pi^0$  and  $\eta$  mesons.  $\omega$ ,  $\eta'$  etc. also contribute to the decay photon spectrum, marginally. Subtraction of the decay background from inclusive photon spectrum is a very challenging task. WA98 Collaboration [11] used the subtraction method using invariant mass analysis for decay background and later PHENIX Collaboration [12] has developed this method to a much higher level of sophistication.

### Invariant mass analysis

Extraction of direct photon spectrum from the inclusive photon spectrum is done using invariant mass analysis as the primary step. First of all, all the detected photons are listed on an event by event basis. Then by selecting two photons randomly from an event, invariant mass of the pair is calculated. If  $E_1$ ,  $E_2$  are the energies and  $\mathbf{p}_1$ ,  $\mathbf{p}_2$  are the three momentum of the photons respectively, then the invariant mass of the pair is,

$$M_{\gamma\gamma} = [(E_1 + E_2)^2 - (\mathbf{p}_1 + \mathbf{p}_2)^2]^{1/2}. \quad (1)$$

If the value of  $M_{\gamma\gamma}$  is close to  $m_{\pi^0}$ , it is assumed that they are the decay products from the same pion and a  $\pi^0$  spectrum is obtained. Similarly the  $\eta$  spectrum is obtained. These two spectra are then used to determine the decay photon spectrum using kinematics and the subtraction of this spectrum from the inclusive spectrum gives the direct photon spectrum.

However, in an event having N number of photons, the total number of photon pairs that can be formed is  ${}^N C_2$ . For large values of N, this number gets very large. Thus, there is a very high probability of getting a pair of

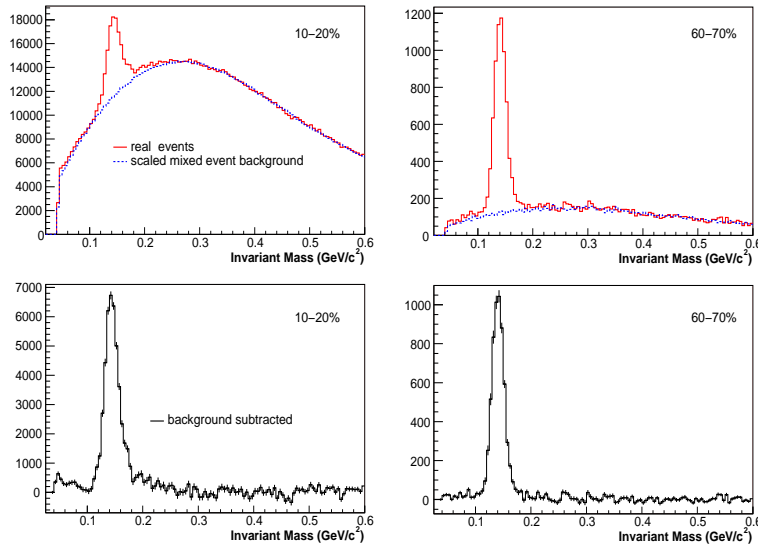


**Fig. 2.** Invariant mass distributions of pairs of electromagnetic clusters passing photon selection cuts for pair transverse momenta satisfying  $3.0 < 3.5$  GeV. Top panels:  $m_{\gamma\gamma}$  distributions in  $Au + Au$  events compared to a normalized mixed-event sample representing the combinatoric background. Bottom panels: The  $m_{\gamma\gamma}$  distributions after subtraction of the combinatoric background for 10-20% and 60-70% centrality bins [13].

photons having an invariant mass  $m_{\pi^0}$  or  $m_{\eta}$ , which are not decay product of the same pion or eta meson.

Several other issues also need to be accounted for: (i) the detector resolution is finite, (ii) the opening angle between the decay photons can get very small, specially if the energy of the pion is large, (iii) the photons may not deposit all their energy in the detector, and (iv) one of the photons may be outside the coverage of the detector.

### Mixed event analysis

Thus, the major problem of invariant mass analysis is that, the accidental (false) photon pairs can also give rise to pion mass and it is not possible to distinguish them from the correlated pairs. To overcome this problem, a mixed event analysis [13] procedure has been used successfully. The basic idea of mixed event technique is to compare particle spectrum from one event to the result for particle combinations from different events, which are *a priori* not correlated. As a first step, properly normalized mixed events are constructed by randomly sampling photons from different events. The difference of the invariant mass spectra (see Fig. 2) of the real events and the mixed events then

gives the pion and  $\eta$  distributions. Once again, the decay photon spectrum is subtracted from the inclusive photon spectrum to get the direct photons.

### Internal conversion and tagging of decay photons

An alternative approach of separating direct photons from decay background is by measuring the ‘quasi-real’ virtual photons which appear as low mass electron positron pair. It is assumed that, any source of real photons also produces low mass virtual photons which decay into  $e^+e^-$  pair. This method is known as internal conversion method [14] and is based on two assumptions. The first assumption is that the ratio of direct to inclusive photons is the same for real as well as virtual photons having  $m_\gamma < 30$  MeV, i.e,  $\gamma_{\text{dir}}^*/\gamma_{\text{incl}}^* = \gamma_{\text{dir}}/\gamma_{\text{incl}}$ . Secondly, the mass distribution follows the Kroll-Wada formula [15]:

$$\frac{d^2 n_{ee}}{dm_{ee}} = \frac{2\alpha}{3\pi} \frac{1}{m_{ee}} \sqrt{1 - \frac{4m_e^2}{m_{ee}^2}} \left(1 + \frac{2m_e^2}{m_{ee}^2}\right) S dn_\gamma. \quad (2)$$

Here,  $m_e$  and  $m_{ee}$  are the masses of electron and  $e^+e^-$  pair respectively and  $\alpha$  is the fine structure constant. This method is used for Compton scattering ( $q + g \rightarrow q + \gamma^* \rightarrow q + e^+ + e^-$ ), Dalitz decay ( $\pi^0, \eta \rightarrow e^+e^-\gamma$ ,  $\omega \rightarrow e^+e^-\pi^0$ ) and also for two  $\gamma$  decay of several other hadrons. The factor S in Eqn. (2) is process dependent and for  $\pi^0$  ( $\rightarrow \gamma\gamma^* \rightarrow \gamma e^+e^-$ ) decay it is expressed as [16]:

$$S = |F(m_{ee}^2)|^2 \left(1 - \frac{m_{ee}^2}{M_h^2}\right)^3, \quad (3)$$

where,  $M_h$  is the hadron mass and  $F(m_{ee}^2)$  is the form factor. The factor S is 0 for  $m_{ee} > M_h$  and goes to 1 as  $m_{ee} \rightarrow 0$  or  $m_{ee} \ll p_T$ . The key advantage of this method is the greatly improved signal to background ratio which is achieved by elimination of the contribution of Dalitz ( $\pi^0$ ) decay. The experimentally measured quantity is the ratio of  $e^+e^-$  pairs in a particular invariant mass bin and the direct photon spectrum is obtained by multiplying  $\gamma_{\text{dir}}^*/\gamma_{\text{incl}}^*$  to the measured inclusive photon spectrum (left panel of Fig 3).

Due to the excellent resolution of the PHENIX detector to measure charged particles at low momenta, another powerful technique known as ‘tagging of decay photons’ [17] is used to eliminate the  $\pi^0$  decay background. This method is very useful in the low and intermediate  $p_T$  range ( $1 < p_T < 5$  GeV) as the systematic uncertainties introduced by detector efficiency, acceptance etc. cancel out for measuring  $\gamma/\gamma_{\pi^0}$  directly in-place of conventional double ratio ( $R = (\gamma/\pi^0)_{\text{measured}}/(\gamma/\pi^0)_{\text{decay}}$ ) technique. In this method, the invariant mass ( $m_{\gamma e^+ e^-}$ ) distribution of the  $\pi^0$  ( $\rightarrow \gamma\gamma^* \rightarrow \gamma e^+e^-$ ) decay products is constructed and then mixed event analysis is used for the final subtraction (middle and right panel of Fig 3).

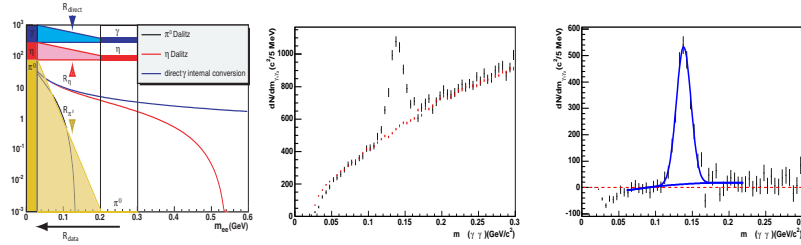


**Fig. 3.** Left Panel: Invariant mass distribution of virtual photons from  $\pi^0$  and  $\eta$  Dalitz decay as well as from direct photons [14]. Middle and right panels: Invariant mass spectrum in ‘tagging’ of decay photon method [17].

### 2.3 Sources of direct photons

Direct photons can be classified into different categories depending on their origin from different stages of the expanding fireball formed after the collision. These are: (1) prompt photons, which originate from initial hard scatterings, (2) pre-equilibrium photons, produced before the medium gets thermalized, (3) thermal photons from quark-gluon plasma as well as by hadronic reactions in the hadronic phase, and (4) photons from passage of jets through plasma. It is not possible experimentally to distinguish between the different sources. Thus, theory can be used with a great advantage to identify these sources of direct photons and their relative importance in the spectrum [18].

#### Partonic processes for production of prompt photons

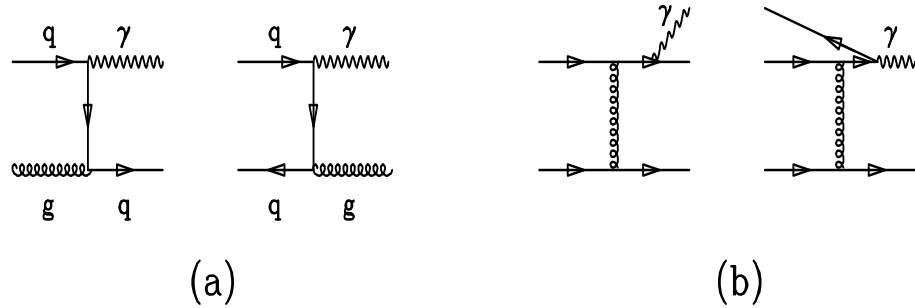


**Fig. 4.** Partonic processes for production of photons from (a) quark gluon Compton scattering, quark anti-quark annihilation process and (b) quark fragmentation.

In relativistic heavy ion collisions, prompt photons are produced due to quark gluon Compton scattering ( $q + g \rightarrow g + \gamma$ ), quark anti-quark annihilation process ( $q + \bar{q} \rightarrow g + \gamma$ ), and quark fragmentation ( $q \rightarrow q + \gamma$ ) following

scattering of partons of the nucleons in the colliding nuclei (see Fig 4). At lowest order in  $\alpha\alpha_s$ , quark gluon Compton scattering and quark anti-quark annihilation processes dominate the photon production. In Next to Leading Order (NLO) calculation, many more complicated scattering processes appear in the photon production cross-section and the total contribution can be written as addition of two different terms as [19],

$$\frac{d\sigma}{d\vec{p}_T d\eta} = \frac{d\sigma^{(D)}}{d\vec{p}_T d\eta} + \frac{d\sigma^{(F)}}{d\vec{p}_T d\eta} \quad (4)$$

In the above equation ‘D’ stands for ‘Direct’ or the total Compton scattering and annihilation contribution while the photons from fragmentation are denoted by ‘F’. It is clear that the ‘D’ photons are well separated from hadrons. The ‘F’ photons on the other hand have their origin in collinear fragmentation of coloured high  $p_T$  partons and are accompanied by hadrons. This can be used with advantage as the produced photons can be separated out by employing useful isolation cuts. The two terms in Eqn. (4) can be written explicitly as [20]:

$$\begin{aligned} \frac{d\sigma^{(D)}}{d\vec{p}_T d\eta} &= \sum_{i,j=q,\bar{q},g} \int dx_1 dx_2 F_{i/h_1}(x_1, M) F_{j/h_2}(x_2, M) \frac{\alpha_s(\mu_R)}{2\pi} \\ &\times \left( \frac{d\hat{\sigma}_{ij}}{d\vec{p}_T d\eta} + \frac{\alpha_s(\mu_R)}{2\pi} K_{ij}^{(D)}(\mu_R, M, M_F) \right) \end{aligned} \quad (5)$$

and

$$\begin{aligned} \frac{d\sigma^{(F)}}{d\vec{p}_T d\eta} &= \sum_{i,j,k=q,\bar{q},g} \int dx_1 dx_2 \frac{dz}{z^2} F_{i/h_1}(x_1, M) F_{j/h_2}(x_2, M) D_{\gamma/k}(z, M_F) \\ &\times \left( \frac{\alpha_s(\mu_R)}{2\pi} \right)^2 \left( \frac{d\hat{\sigma}_{ij}^k}{d\vec{p}_T d\eta} + \frac{\alpha_s(\mu_R)}{2\pi} K_{ij,k}^{(F)}(\mu_R, M, M_F) \right). \end{aligned} \quad (6)$$

Here  $F_{i/h_{1,2}}(x, M)$  are the parton distribution functions and  $\alpha_s(\mu_R)$  is the strong coupling defined in the  $\overline{MS}$  renormalization scheme at the renormalization scale  $\mu_R$ . For details see Ref. [19]. As mentioned earlier, in a complete and consistent NLO pQCD [ $O(\alpha\alpha_s^2)$ ] calculation important contribution to prompt photon result arises from various possible  $2 \rightarrow 3$  process like  $ab \rightarrow \gamma cd$  for the Direct as well as for the Fragmentation processes [20, 21].

In case of photons from fragmentation, the higher order correction is very important at low  $x_T$  ( $= 2p_T/\sqrt{s}$ ). By choosing a scale for factorization, renormalization, and fragmentation, all equal to  $p_T/2$ , a very good quantitative description is obtained for all the available  $pp$  and  $p\bar{p}$  data without introduction of any intrinsic  $k_T$ . Results spanning over two orders of magnitude in energy and over nine orders of magnitude in cross sections, are shown in Fig. 5.

It should be mentioned though, that a similar exercise for pions requires a scale of  $p_T/3$  [22].

In the early calculations, the results for nucleus-nucleus scatterings were often obtained by multiplying the  $pp$  results for some  $\sqrt{s}$  with corresponding scaling factor  $N_{\text{coll}}$  ( $= \sigma_{NN} T_{AB}$ ; where,  $\sigma_{NN}$  is the nucleon-nucleon cross-section and  $T_{AB}$  is the nuclear overlapping function for nuclei A and B) or number of binary collisions. In actual practice, often enough,  $\sigma_{NN}$  was replaced by  $\sigma_{pp}$ . However, as the valence quark structures of protons ( $uud$ ) and neutrons ( $udd$ ) are different, one needs to correctly account for the iso-spin of the nucleons to calculate the prompt contribution. This correction will strongly affect the results in the  $p_T$  range, where the valence quark contribution is significant. Also, remember that there is no direct measurement for  $pn$  and  $nn$  cross-sections, though they can be estimated by comparing results of scatterings involving deuterons. The effect of shadowing on structure function and energy loss of final state quarks before they fragment into hadrons are two other corrections [23] which need to be accounted for.

In order to clearly see this point we show the results for prompt photons for  $nn$  and  $pn$  collisions normalized to those for  $pp$  collisions at  $\sqrt{s} = 200$  GeV in the left panel of Fig. 6. It is clear that at low  $x_T$  (where processes involving gluons dominate) the effect is not very significant, however with larger values of  $x_T$  (where the processes involving valence quarks dominate), the production of photons decreases by a large factor for the case of  $pn$  and  $nn$  collisions.

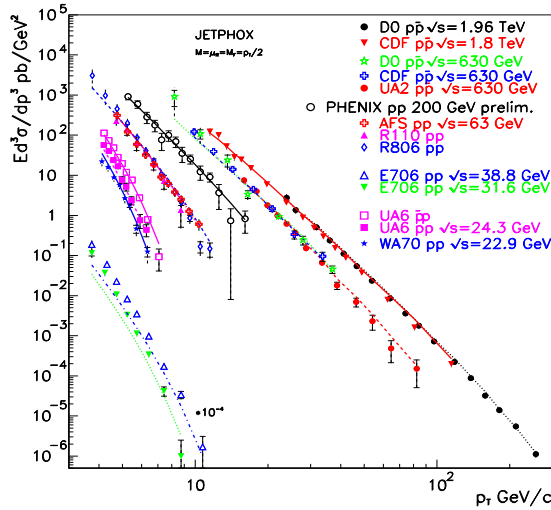


**Fig. 5.** World's inclusive and isolated direct photon production cross-sections measured in  $pp$  and  $p\bar{p}$  collisions compared to JETPHOX NLO predictions, using BFG II(CTEQ6M) for fragmentation (structure) functions and a common scale  $p_T/2$  [19].



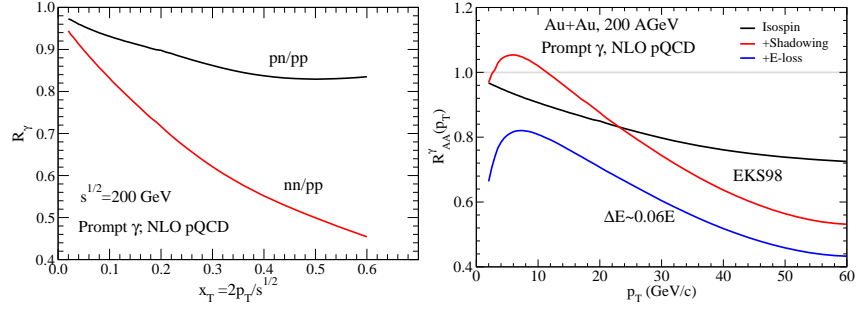


**Fig. 6.** Left panel: Prompt photons for  $pn$  and  $nn$  collisions normalized to those for  $pp$  collisions at  $\sqrt{s} = 200$  GeV. Right panel: Iso-spin, shadowing and energy loss corrected  $R_{AA}$  for prompt photons at 200A GeV  $Au + Au$  collisions using NLO pQCD.

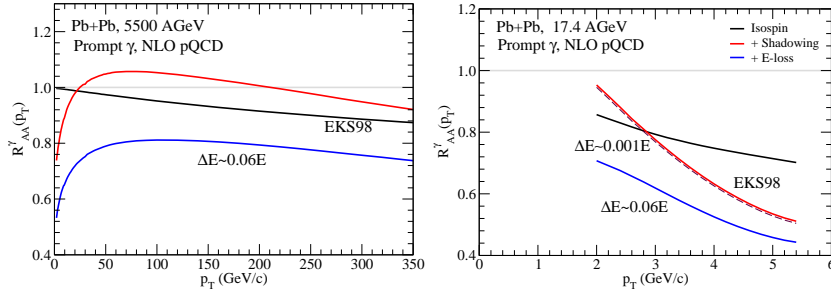


**Fig. 7.** Iso-spin, shadowing and energy-loss corrected  $R_{AA}$  for prompt photons at LHC (left panel) and SPS (right panel) energies using NLO pQCD.

The transverse momentum dependent nuclear modification factor  $R_{AA}$ , defined as,

$$R_{AA}(p_T) = \frac{1}{N_{\text{coll}}} \frac{d\sigma_{\gamma}^{AA}(p_T)/dyd^2p_T}{d\sigma_{\gamma}^{pp}(p_T)/dyd^2p_T} \quad (7)$$

for prompt photons using NLO pQCD and considering iso-spin, shadowing and energy-loss effects for 200A GeV  $Au + Au$  collisions at RHIC is shown in the right panel of Fig. 6. We note that, for  $p_T < 10$  GeV, the iso-spin and shadowing corrected result shows an enhancement in the prompt photon production compared to the situation when only the iso-spin correction is incorporated [24]. This is due to anti-shadowing for larger values of Bjorken  $x$  or large  $x_T$ . The inclusion of the energy-loss pushes down the value of  $R_{AA}$  to less than one for all  $p_T$ . We also give a comparison with the PHENIX [25] experimental data in the bottom lower panel of Fig. 8.

NLO results at LHC ( $Pb + Pb@5.5A$  TeV) and SPS ( $Pb + Pb@17.4A$  GeV) are shown in Fig. 7. To clearly demonstrate the relative features of iso-

spin, shadowing and energy-loss corrected prompt photons at different collider energies, results for  $R_{AA}$  as function of  $x_T$  are shown in Fig. 8.

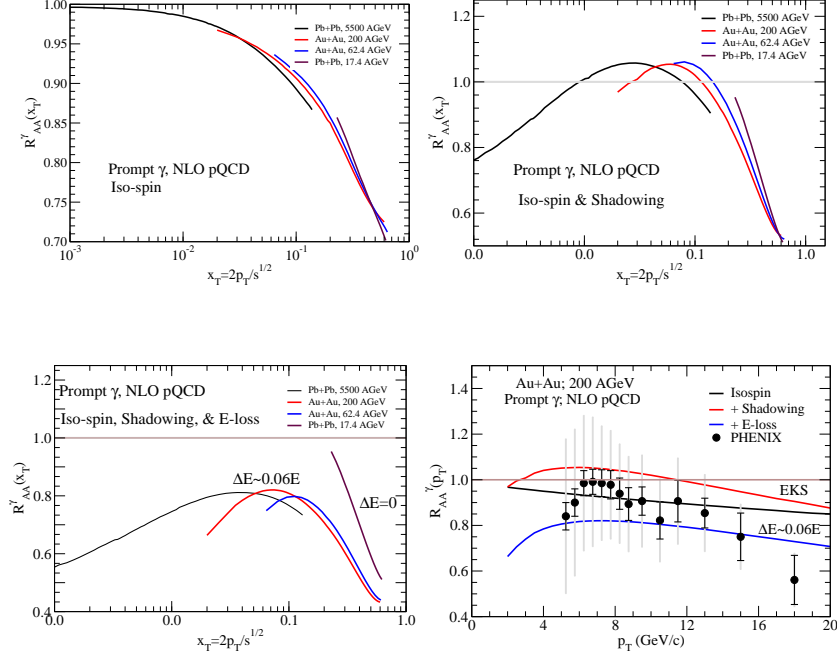


**Fig. 8.** Iso-spin, shadowing and fragmentation energy-loss corrected NLO pQCD results at different collider energies with different target projectile combination and comparison of the RHIC results with PHENIX [25] data.

## 2.4 Photon production from Quark-Gluon Plasma

The thermal emission rate of photons with energy  $E$  and momentum  $p$  from a small system (compared to the photon mean free path) is related to the imaginary part of photon self energy by the following relation

$$E \frac{dR}{d^3p} = \frac{-2}{(2\pi)^3} \text{Im} \Pi_\mu^{R,\mu} \frac{1}{e^{E/T} - 1} \quad (8)$$

where,  $\Pi_\mu^{R,\mu}$  is the retarded photon self-energy at a finite temperature  $T$ . This relation is valid in the perturbative [26] as well as non-perturbative [27] limits. It is also valid to all orders in the strong interactions and to order  $e^2$  in the electromagnetic interactions. If the photon self-energy is approximated by carrying out a loop expansion to some finite order, then the formulation of Eqn. (8) is equivalent to relativistic kinetic theory. In order to illustrate this, we closely follow the treatment of Ref. [28].

Thus using relativistic kinetic theory formulation, the contribution of these processes to the rate can be written as [28, 29]:

$$\begin{aligned} \mathcal{R}_i = \mathcal{N} \int \frac{d^3 p_1}{2E_1(2\pi)^3} \frac{d^3 p_2}{2E_2(2\pi)^3} f_1(E_1) f_2(E_2) (2\pi)^4 \delta(p_1^\mu + p_2^\mu - p_3^\mu - p^\mu) \\ \times |\mathcal{M}_i|^2 \frac{d^3 p_3}{2E_3(2\pi)^3} \frac{d^3 p}{2E(2\pi)^3} [1 \pm f_3(E_3)] \end{aligned} \quad (9)$$

where  $\mathcal{M}_i$  represents the amplitude for one of these processes and the  $f$ 's are the Fermi-Dirac or Bose-Einstein distribution functions as appropriate. Positive and negative signs in the last part of Eqn. (9) correspond to Bose enhancement and Pauli suppression respectively.

The integral above can be simplified by introducing Mandelstam variables  $s = (p_1 + p_2)^2$ ,  $t = (p_1 - p_3)^2$  and  $u = (p_1 - p)^2$ . Now the differential photon rate can be written as:

$$\begin{aligned} E \frac{d\mathcal{R}_i}{d^3 p} = \frac{\mathcal{N}}{(2\pi)^7} \frac{1}{16E} \int ds dt |\mathcal{M}_i(s, t)|^2 \int dE_1 dE_2 f_1(E_1) f_2(E_2) \\ \times [1 \pm f_3(E_1 + E_2 - E)] \theta(E_1 + E_2 - E) (aE_1^2 + bE_1 + c)^{-1/2} \end{aligned} \quad (10)$$

where,

$$\begin{aligned} a &= -(s + t)^2, \\ b &= 2(s + t)(Es - E_2t), \\ c &= st(s + t) - (Es + E_2t)^2. \end{aligned} \quad (11)$$

Considering the photon energy to be large, one can consider,  $f_1(E_1) f_2(E_2) \approx e^{-(E_1 + E_2)/T}$  and simplify the above as

$$E \frac{d\mathcal{R}_i}{d^3 p} = \frac{\mathcal{N}}{(2\pi)^6} \frac{T}{32E} e^{-E/T} \int \frac{ds}{s} \ln(1 \pm e^{-s/4ET})^{\pm 1} \int dt |\mathcal{M}_i(s, t)|^2 \quad (12)$$

In the above equation, positive and negative signs stand for fermions ( $q$ ) and bosons ( $g$ ) in the final state respectively.

The relation between the amplitude and differential cross-section for massless particles can be written as,

$$\frac{d\sigma}{dt} = \frac{|\mathcal{M}|^2}{16\pi s^2} \quad (13)$$

And thus, the differential cross-sections for annihilation process and Compton scattering are:

$$\frac{d\sigma^{\text{annihilation}}}{dt} = \frac{8\pi\alpha\alpha_s}{9s^2} \frac{u^2 + t^2}{ut} \quad (14)$$

and

$$\frac{d\sigma^{\text{Compton}}}{dt} = \frac{-\pi\alpha\alpha_s}{3s^2} \frac{u^2 + s^2}{us} \quad (15)$$

For annihilation process,  $\mathcal{N} = 20$  when summing over  $u$  and  $d$  quarks and for Compton scattering  $\mathcal{N} = 320/3$ . The total cross-section can be obtained after integrating over  $t$ . These differential cross sections have a singularity at  $t$  and/or  $u = 0$  and the total cross-section is infinite as the processes involve exchange of mass-less particle.

To screen this divergence many-body effects are necessary. This approach will be discussed later. As a first step let us isolate the region of phase space causing the divergences. The integration is done over

$$-s + k_c^2 \leq t \leq -k_c^2, \quad 2k_c^2 \leq s \leq \infty, \quad (16)$$

where  $T^2 \gg k_c^2 > 0$  is an infrared cut-off.

This treats  $u$  and  $t$  symmetrically and maintains the identity  $s + t + u = 0$  appropriate for all massless particles.

In the limit that  $k_c^2 \rightarrow 0$ ,

$$E \frac{d\mathcal{R}^{\text{Compton}}}{d^3p} = \frac{5}{9} \frac{\alpha\alpha_s}{6\pi^2} T^2 e^{-E/T} [\ln(4ET/k_c^2) + C_F] \quad (17)$$

$$E \frac{d\mathcal{R}^{\text{annihilation}}}{d^3p} = \frac{5}{9} \frac{\alpha\alpha_s}{3\pi^2} T^2 e^{-E/T} [\ln(4ET/k_c^2) + C_B] \quad (18)$$

where

$$C_F = \frac{1}{2} - C_{\text{Euler}} + \frac{12}{\pi^2} \sum_{n=2}^{\infty} \frac{(-1)^n}{n^2} \ln n = 0.0460\dots\dots, \quad (19)$$

$$C_B = -1 - C_{\text{Euler}} - \frac{6}{\pi^2} \sum_{n=2}^{\infty} \frac{1}{n^2} \ln n = -2.1472\dots\dots \quad (20)$$

These expressions use the full Fermi-Dirac or Bose-Einstein distribution functions in the final state.

These results have a very interesting structure. Thus, the factor  $5/9$  arises from the sum of the squares of the electric charges of the  $u$  and  $d$  quarks, the factor  $\alpha\alpha_s$  comes from the topological structure of the diagrams, a factor  $T^2$  comes from phase space which gives the overall dimension of the rate, and we have the Boltzmann factor  $e^{-E/T}$  for photons of energy  $E$ . The logarithm arises due to the infrared behavior.

### Infrared contribution

The infrared divergence in the photon production rate [28] discussed above is caused by a diverging differential cross-section when the momentum transfer

goes to zero. Often-times long-ranged forces can be screened by many-body effects at finite temperatures. Braaten and Pisarski have analyzed problems such as this one in QCD [30]. They have argued that a cure can be found in reordering perturbation theory by expanding correlation functions in terms of effective propagators and vertices instead of bare ones. These effective propagators and vertices are just the bare ones plus one-loop corrections, with the caveat that the one-loop corrections are evaluated in the high temperature limit. This makes them relatively simple functions.

The analysis of Braaten and Pisarski shows that a propagator must be dressed if the momentum flowing through it is soft (small compared to  $T$ ). This is because propagation of soft momenta is connected with infrared divergences in loops. Dressing of propagators are necessary, otherwise corrections due to these are also infinite.

Using the one loop corrected propagators and vertices and the contribution to the rate coming from the infrared sensitive part of phase space can be written as,

$$E \frac{d\mathcal{R}^{\text{BP}}}{d^3p} = \frac{5}{9} \frac{\alpha\alpha_s}{2\pi^2} T^2 e^{-E/T} \ln\left(\frac{k_c^2}{2m_q^2}\right) \quad (21)$$

where,  $2m_q^2 = \frac{1}{3}g^2T^2$ .

Adding this contribution to those given by Eqns. (19) and (20), the final result can be written as;

$$E \frac{d\mathcal{R}}{d^3p} = \frac{5}{9} \frac{\alpha\alpha_s}{2\pi^2} T^2 e^{-E/T} \ln\left(\frac{2.912 E}{g^2 T}\right). \quad (22)$$

This is independent of cut-off  $k_c$ . Thus, the Braaten-Pisarski method has worked beautifully to shield the singularity encountered above. We also note that in kinetic theory calculation, the effective infrared cutoff is  $k_c^2 = 2m_q^2$ . In earlier works an infrared cut-off was often imposed by giving the exchanged quark an effective temperature-dependent mass.

These early results have been brought to a high degree of sophistication and results complete to leading order in  $\alpha_s$  with inclusion of LPM effects are now available, which should be used for detailed calculation [31].

### Photons from passage of jets through QGP

The relativistic heavy ion collisions at RHIC (and LHC) energies are marked by a large production of high energy quark and gluon jets which lose energy while passing through the QGP due to collision and radiation of gluons. This is the celebrated phenomenon of jet-quenching. A quark jet having a transverse momentum  $p_T$  would be formed within  $\tau \sim 1/p_T$  which can be much smaller than  $\tau_0$ , when QGP is formed, for large  $p_T$ . This quark (or anti-quark) jet, while passing through QGP may annihilate with a thermal anti-quark (or

quark) or undergo a Compton scattering with a thermal gluon and lead to production of a high energy photon. This process is called the jet-photon conversion [9].

We have seen that the kinematics of the annihilation of a quark anti-quark pair ( $q + \bar{q} \rightarrow \gamma + g$ ) is expressed in terms of the Mandelstam variables  $s = (p_q + p_{\bar{q}})^2$ ,  $t = (p_q - p_\gamma)^2$  and  $u = (p_{\bar{q}} - p_\gamma)^2$ . We also recall that the largest contribution to the production of photons arises from small values of  $t$  or  $u$ , corresponding to  $p_\gamma \sim p_q$  or  $p_\gamma \sim p_{\bar{q}}$  [2, 9, 32].

The phase-space distribution of the quarks and gluons produced in a nuclear collision can be approximately decomposed into two components, a thermal component  $f_{\text{th}}$  characterized by a temperature  $T$  and a hard component  $f_{\text{jet}}$  given by hard scattering of the partons and limited to transverse momenta  $p_T \gg 1$  GeV:  $f(\mathbf{p}) = f_{\text{th}}(\mathbf{p}) + f_{\text{jet}}(\mathbf{p})$ .  $f_{\text{jet}}$  dominates for large momenta, while at small momenta  $f$  is completely given by the thermal part.

The phase space distribution for the quark jets propagating through the QGP is given by the perturbative QCD result for the jet yield [9]:

$$f_{\text{jet}}(\mathbf{p}) = \frac{1}{g_q} \frac{(2\pi)^3}{\pi R_\perp^2 \tau p_T} \frac{dN_{\text{jet}}}{d^2 p_T dy} R(r) \delta(\eta - y) \Theta(\tau_{\text{max}} - \tau_i) \Theta(R_\perp - r) \quad (23)$$

where  $g_q = 2 \times 3$  is the spin and colour degeneracy of the quarks,  $R_\perp$  is the transverse dimension of the system, and the  $\eta$  is the space-time rapidity.  $R(r)$  is a transverse profile function.  $\tau_{\text{max}}$  is the smaller of the lifetime  $\tau_f$  of the QGP and the time  $\tau_d$  taken by the jet produced at position  $\mathbf{r}$  to reach the surface of the plasma.

One can approximate the invariant photon differential cross sections for the annihilation process and Compton scattering as [2, 9],

$$E_\gamma \frac{d\sigma^{(a)}}{d^3 p_\gamma} \sim \sigma^{(a)}(s) \frac{1}{2} E_\gamma [\delta(\mathbf{p}_\gamma - \mathbf{p}_q) + \delta(\mathbf{p}_\gamma - \mathbf{p}_{\bar{q}})], \quad (24)$$

and

$$E_\gamma \frac{d\sigma^{(C)}}{d^3 p_\gamma} \sim \sigma^{(C)}(s) E_\gamma \delta(\mathbf{p}_\gamma - \mathbf{p}_q) \quad (25)$$

Here  $\sigma^{(a)}(s)$  and  $\sigma^{(C)}(s)$  are the corresponding total cross sections.

Using Eqn. (24) and Eqn. (25), the rate of production of photons due to annihilation and Compton scattering are given by [2]:

$$\begin{aligned} E_\gamma \frac{dN^{(a)}}{d^4 x d^3 p_\gamma} &= \frac{16 E_\gamma}{2(2\pi)^6} \sum_{q=1}^{N_f} f_q(\mathbf{p}_\gamma) \int d^3 p f_{\bar{q}}(\mathbf{p}) [1 + f_g(\mathbf{p})] \sigma^{(a)}(s) \\ &\times \frac{\sqrt{s(s-4m^2)}}{2E_\gamma E} + (q \leftrightarrow \bar{q}) \end{aligned} \quad (26)$$

$$\begin{aligned}
E_\gamma \frac{dN^{(C)}}{d^4x d^3p_\gamma} &= \frac{16E_\gamma}{(2\pi)^6} \sum_{q=1}^{N_f} f_q(\mathbf{p}_\gamma) \int d^3p f_g(\mathbf{p}) [1 - f_q(\mathbf{p})] \sigma^{(C)}(s) \\
&\times \frac{(s - m^2)}{2EE_\gamma} + (q \rightarrow \bar{q})
\end{aligned} \tag{27}$$

The  $f$ 's are the distribution functions for the quarks, anti-quarks and gluons. Inserting thermal distributions for the gluons and quarks one can obtain an analytical expression for these emission rates for an equilibrated medium [2, 28, 29].

In order to estimate the jet photon conversion contribution, we first note that, the integrals over  $\mathbf{p}$  in Eqns. (26) and (27) are dominated by small momenta. Therefore dropping the jet part in the distributions,  $f(\mathbf{p})$  in the integrands is approximated by the thermal part. Now performing the integrals and identifying the quark and anti-quark distributions outside the integrals with the jet distributions, results for Compton and annihilation scatterings due to jet-conversions are given as,

$$\begin{aligned}
E_\gamma \frac{dN_\gamma^{(a)}}{d^3p_\gamma d^4x} &= E_\gamma \frac{dN_\gamma^{(C)}}{d^3p_\gamma d^4x} \\
&= \frac{\alpha\alpha_s}{8\pi^2} \sum_{f=1}^{N_f} \left(\frac{e_{qf}}{e}\right)^2 [f_q(\mathbf{p}_\gamma) + f_{\bar{q}}(\mathbf{p}_\gamma)] T^2 \left[\ln\left(\frac{4E_\gamma T}{m^2}\right) + C\right]
\end{aligned} \tag{28}$$

Here,  $C = -1.916$ . If we include three lightest quark flavours, then  $\sum_f e_{qf}^2/e^2 = 2/3$ . We also assume that the mass  $m$  introduced here to shield the infrared divergence can be identified with the thermal quark mass  $m_{th}$ .

These pioneering works have now been corrected for energy loss and flavour change suffered by the jets, as they pass through the plasma [33] as well as bremsstrahlung induced by the passage of the jets through the plasma [34].

### Equilibration time for photons

It is of interest to get an idea about the equilibration time of photons in the medium. Following the treatment of Ref. [28], we note that the six-dimensional phase space distribution  $dn/d^3p (= dN/d^3x d^3p)$ , for the photons satisfies the rate equation:

$$\frac{d}{dt} \left( \frac{dn}{d^3p} \right) = \frac{dR}{d^3p} \left( 1 - \frac{dn/d^3p}{dn_{eq}/d^3p} \right). \tag{29}$$

In the above equation,  $dn_{eq}/d^3p$  is the equilibrium distribution and is expressed as Planck's distribution,

$$\frac{dn^{eq}}{d^3p} = \frac{2}{(2\pi)^3} \frac{1}{e^{E/T} - 1}. \tag{30}$$

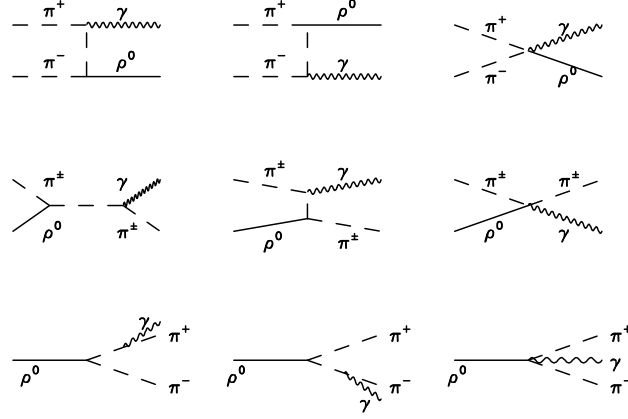


**Fig. 9.** Typical hadronic reactions for photon production.

Considering  $\tau_{\text{eq}} (= \frac{dn_{\gamma}^{\text{eq}}}{d^3p} / \frac{dR}{d^3p})$  as the time for equilibration and assuming zero photons at the beginning we can write,

$$\frac{dn}{d^3p} = \frac{dn^{\text{eq}}}{d^3p} \left(1 - e^{t/\tau_{\text{eq}}}\right). \quad (31)$$

Using the rate equation, the thermalization time can be expressed in a simplified form (considering  $E > 2T$ ) as:

$$\tau_{\text{eq}} = \frac{9E}{10\pi\alpha\alpha_s T^2} \frac{1}{\ln\left(\frac{2.9E}{g^2 T} + 1\right)}. \quad (32)$$

For energy values  $E = 0.5, 1, 2, 3$  GeV, corresponding values for  $\tau_{\text{eq}}$  will be about 270, 356, 505, 639 fm/c respectively, when the temperature is 200 MeV. As the life time of the system is very short, of the order of few tens of fm/c, it is very clear that the high energy photons will never reach the equilibrium state in heavy ion collisions. This is an important confirmation for the validity of the assumption made in all such studies that photons, once produced in the collision, leave the system with out any further re-interaction.

## 2.5 Photons from hot hadronic matter

Hot hadronic matter produced after the hadronization of the quark-gluon plasma will also lead to production of photons due to hadronic reactions. These photons will dominate the spectrum at lower  $p_T$  ( $< 1$  GeV). The first ever calculation of production of thermal photons from hadronic matter was performed by Kapusta *et al.* [28].

In a hot hadronic gas (having temperature of the order of pion mass), the most important hadronic constituents for photon production are  $\pi$  and



$\rho$  mesons (see Fig. 9). The low mass of pions and the large spin iso-spin degeneracy of  $\rho$  mesons, make them the most easily accessible particles in the medium. In order to illustrate the photon production from these two mesons, we closely follow the treatment of KLS [28]. In a hadronic reaction involving charged  $\pi$  and  $\rho$  meson, the typical Lagrangian describing the interaction can be written as:

$$\mathcal{L} = |D_\mu \Phi|^2 - m_\pi^2 |\Phi|^2 - \frac{1}{4} \rho_{\mu\nu} \rho^{\mu\nu} + \frac{1}{2} m_\rho^2 \rho_\mu \rho^\mu - \frac{1}{4} F_{\mu\nu} F^{\mu\nu} \quad (33)$$

where,

$$D_\mu = \partial_\mu - ieA_\mu - ig_\rho \rho_\mu,$$

$\Phi$  is the complex pion field,  $\rho_{\mu\nu}$  is the  $\rho$  field strength and  $F_{\mu\nu}$  is the photon field tensor. The differential cross-sections for the dominating photon producing processes ( $\pi\rho \rightarrow \pi\gamma$ ) in the hadronic phase is expressed as [28],

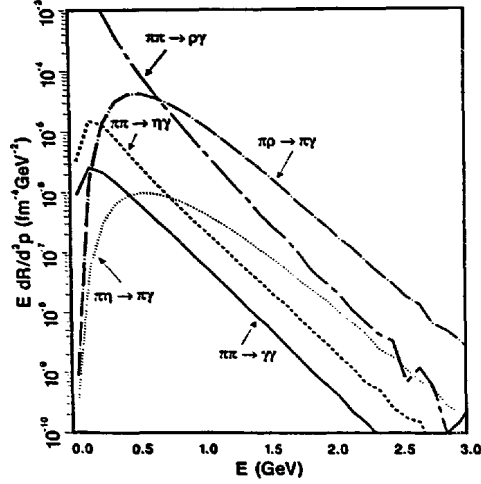


**Fig. 10.** Left Panel: Yield of photons from different hadronic channels (taken from [28]).

$$\frac{d\sigma}{dt}(\pi^+ \rho^0 \longrightarrow \pi^+ \gamma) = \frac{d\sigma}{dt}(\pi^- \rho^0 \longrightarrow \pi^- \gamma)$$

$$\begin{aligned}
&= \frac{\alpha g_\rho^2}{12sp_{c.m.}^2} \left[ 2 - \frac{(m_\rho^2 - 4m_\pi^2)s}{(s - m_\pi^2)^2} - (m_\rho^2 - 4m_\pi^2) \right. \\
&\quad \left. \times \left( \frac{s - m_\rho^2 + m_\pi^2}{s - m_\pi^2} \frac{1}{u - m_\pi^2} + \frac{m_\pi^2}{(u - m_\pi^2)^2} \right) \right]. \quad (34)
\end{aligned}$$

Similarly for

$$\begin{aligned}
\frac{d\sigma}{dt}(\pi^- \rho^+ \rightarrow \pi^0 \gamma) &= \frac{d\sigma}{dt}(\pi^+ \rho^- \rightarrow \pi^0 \gamma) \\
&= -\frac{\alpha g_\rho^2}{48sp_{c.m.}^2} \left[ 4(m_\rho^2 - 4m_\pi^2) \left[ \frac{u}{(u - m_\pi^2)^2} + \frac{t}{(t - m_\rho^2)^2} \right. \right. \\
&\quad \left. \left. - \frac{m_\rho^2}{s - m_\pi^2} \left( \frac{1}{u - m_\pi^2} + \frac{1}{t - m_\rho^2} \right) \right] + \left[ \left( 3 + \frac{s - m_\pi^2}{m_\rho^2} \right) \right. \right. \\
&\quad \left. \left. \times \frac{s - m_\pi^2}{t - m_\rho^2} \right] - \frac{1}{2} + \frac{s}{m_\rho^2} - \left( \frac{s - m_\pi^2}{t - m_\rho^2} \right)^2 \right] \quad (35)
\end{aligned}$$

and also,

$$\begin{aligned}
\frac{d\sigma}{dt}(\pi^0 \rho^+ \rightarrow \pi^+ \gamma) &= \frac{d\sigma}{dt}(\pi^0 \rho^- \rightarrow \pi^- \gamma) \\
&= \frac{\alpha g_\rho^2}{48sp_{c.m.}^2} \left[ \frac{9}{2} - \frac{s}{m_\rho^2} - \frac{4(m_\rho^2 - 4m_\pi^2)s}{(s - m_\pi^2)^2} \right. \\
&\quad \left. + \frac{(s - m_\pi^2)^2 - 4m_\rho^2(m_\rho^2 - 4m_\pi^2)}{(t - m_\rho^2)^2} \right. \\
&\quad \left. + \frac{1}{t - m_\rho^2} \left( 5(s - m_\pi^2) - \frac{(s - m_\pi^2)^2}{m_\rho^2} \right) \right. \\
&\quad \left. - \frac{4(m_\rho^2 - 4m_\pi^2)}{s - m_\pi^2} (s - m_\pi^2 + m_\rho^2) \right] \quad (36)
\end{aligned}$$

In the above set of equations,  $s$ ,  $t$ ,  $u$  are the Mandelstam variables and  $p_{c.m.}$  is the three momentum of the interacting particles in their centre of mass frame. Typical results are shown in Fig. 10.

Xiong *et al.* [36] and Song [37] first introduced the  $\pi\rho \rightarrow a_1 \rightarrow \pi\gamma$  channel for photon production in hadronic phase, whereas baryonic processes and medium modification were included by Alam *et al.* [38, 39]. Several refinements, e.g., inclusion of strange sector, use of massive Yang-Mills theory and t-channel exchange of  $\omega$  mesons, were incorporated by Turbide *et al.* [35]. The last calculation is essentially the state of art result at the moment. Photon spectra considering a complete leading rate from QGP [31] and exhaustive reactions in hadronic matter [28, 35] are shown in Fig. 11.

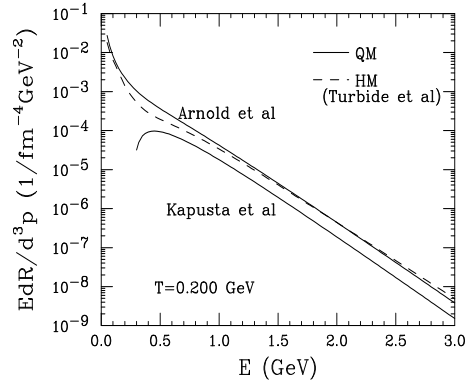


**Fig. 11.** Complete leading order rates from QGP and exhaustive reactions in hadronic matter [28, 31, 35].

### 3 Photons from Pb+Pb@SPS to Au+Au@RHIC

#### 3.1 SPS

In order to get an idea of greatly increased insights provided by single photon production, let us briefly recall some of the important results from the SPS era, many of which preceded the large strides made in our theoretical understanding mentioned above. The first hint of single photon production, which later turned out to be the upper limit of their production, came from the  $S + Au$  collisions studied at the SPS energies [40].

These results were analyzed in two different scenarios by authors of Ref. [41]. In the first scenario, a thermally and chemically equilibrated quark-gluon plasma was assumed to be formed at some initial time ( $\tau_0 \approx 1 \text{ fm}/c$ ), which expanded [42], cooled, and converted into a mixed phase of hadrons and QGP at a phase-transition temperature,  $T_C \approx 160 \text{ MeV}$ . When all the quark-matter was converted into a hadronic matter, the hot hadronic gas continued to cool and expand, and underwent a freeze-out at a temperature of about 140 MeV. The hadronic gas was assumed to consist of  $\pi$ ,  $\rho$ ,  $\omega$ , and  $\eta$  mesons, again in a thermal and chemical equilibrium. This was motivated by the fact that the included hadronic reactions involved [28] these mesons. This was already a considerable improvement over a gas of mass-less pions used in the literature at that time. In the second scenario, the collision was assumed to lead to a hot hadronic gas of the same composition. The initial temperature was determined by demanding that the entropy of the system be determined from the measured particle rapidity density [44]. It was found that the scenario which did not involve a formation of QGP led to a much larger initial temperature and a production of photons which was considerably larger than the upper limit of the photon production, and could be ruled out. The calculation assuming a quark-hadron phase transition yielded results

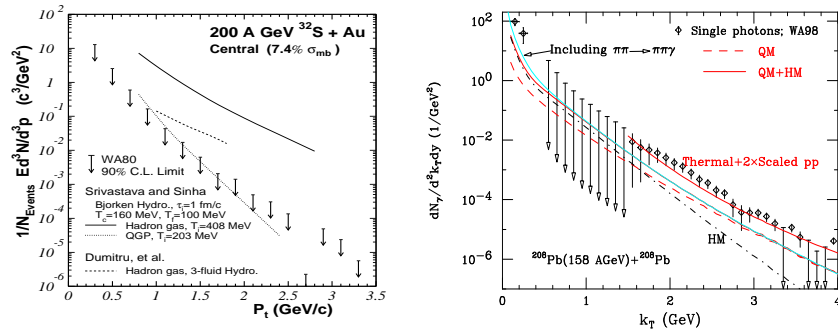


**Fig. 12.** Left panel: Upper limits at the 90 % confidence level on the invariant excess photon yield for the 7.4 %  $\sigma_{mb}$  most central collisions of 200A GeV  $^{32}\text{S} + \text{Au}$  [40]. The solid and the dashed curves give the thermal photon production expected from hot hadron gas calculation [41], while the dotted curve is the calculated thermal photon production expected in the case of a QGP formation. Right panel: Single photon production in  $Pb+Pb$  collision at CERN SPS. Prompt photons are estimated using pQCD (with a K-factor estimated using NLO calculation) and intrinsic  $k_T$  of partons [43].

which were consistent with the upper limit of the photon production. These results were confirmed [45] by several calculations exploring different models of expansion (see left panel of Fig.12).

It was soon realized that one may not limit the hadronic gas to contain just  $\pi$ ,  $\rho$ ,  $\omega$ , and  $\eta$  mesons, as there was increasing evidence that perhaps all the mesons and baryons were being produced in a thermal and chemical equilibrium in such collisions. Thus authors of Ref. [46] explored the consequences of using a hadronic gas consisting of essentially all the hadrons in the Particle Data Book, in a thermal and chemical equilibrium. This led to an interesting result for the  $Pb + Pb$  collision at SPS energies, for which experiments were in progress. It was found that with the rich hadronic gas, the results for the production of photons in the phase-transition and no phase transition models discussed above were quite similar, suggesting that measurement of photons at the SPS energy could perhaps not distinguish between the two cases. However, in a very important observation, it was also noted that the calculations involving hot hadronic gas at the initial time would lead to hadronic densities of several hadrons/ $\text{fm}^3$ , and while those involving a quark gluon plasma in the initial state would be free from this malady. Thus, it was concluded that the calculations involving a phase transition to QGP offered a more natural description.

The WA98 experiment [11], reported the first observation of direct photons in central 158A GeV  $Pb + Pb$  collisions studied at the CERN SPS. This was explained [47] in terms of formation of quark gluon plasma in the initial state (at  $\tau_0 \approx 0.2 \text{ fm}/c$ ), which expanded, cooled and hadronized as in Ref. [46]

(see right panel of Fig. 12). An independent confirmation of this approach was provided by an accurate description [48] of excess dilepton spectrum measured by the NA60 experiment for the same system.

Once again the results for single photons were analyzed by several authors using varying models of expansion as well as rates for production of photons; viz., with or without medium modification of hadronic properties (see, e.g., Ref. [35, 49, 50]). The outcome of all these efforts can be summarized as follows: the single photon production in  $Pb + Pb$  collisions at SPS energies can be described either by assuming a formation of QGP in the initial state or by assuming the formation of a hot hadronic gas whose constituents have massively modified properties. The later description, however, involved a hadronic density of several hadrons/fm<sup>3</sup>, which raises doubts about the applicability of a description in terms of hadrons, as suggested by Ref. [46].

### 3.2 RHIC

The first experimental photon result obtained from the Relativistic Heavy Ion Collider was the centrality dependent single photon data for 200A GeV  $Au + Au$  collisions by PHENIX collaboration [12], where single photons were identified clearly for  $p_T > 4$  GeV. For central collisions, the lower bound on photon transverse momenta was even much lower, upto 2 GeV (Fig. 13). This data was in good agreement with NLO pQCD results for  $pp$  collisions, scaled by number of binary collisions ( without considering the iso-spin effect).

Thermal radiation dominates the direct photon spectrum at lower values of  $p_T$  ( $\leq 3$  GeV) and the measured slope of the thermal photon spectrum can be related to the temperature of the system.

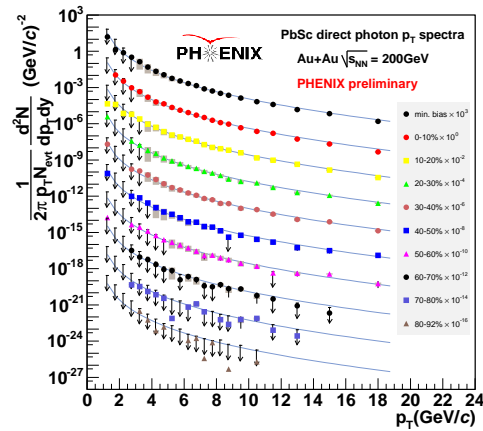


**Fig. 13.** Direct photon results for  $Au + Au$  collisions (left panel) and  $p + p$  collisions (right panel) at  $\sqrt{s_{NN}} = 200A$  GeV [12].

In Fig. 14 results from several theoretical models based on hydrodynamics for thermal photon production at RHIC are shown. The initial temperature and thermalization time for  $Au + Au$  collision at 200A GeV quoted by several theoretical groups [35, 47, 49, 50, 51, 52] are in the range of 450 - 650 MeV and about 0.2 fm/c respectively.

All these calculations are comparable to the experimental data and with each others within a factor of 2 and also confirm the dominance of thermal radiation in the direct photon spectrum in low and intermediate  $p_T$  range.

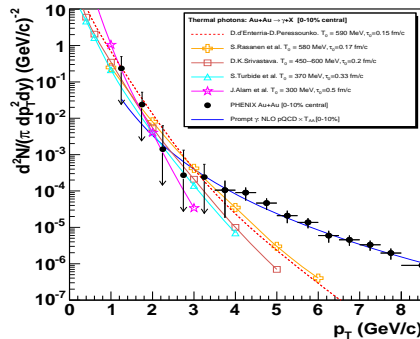


**Fig. 14.** Thermal photon spectra for central 200A GeV  $Au + Au$  collision computed within different models [52] compared to the expected pQCD prompt photon yield and to the experimental total direct photon spectrum measured by PHENIX [25].

### Indications for jet conversion photons

We have already discussed the procedure for calculating the high energy photons due to passage of jets through the quark gluon plasma.

The parametrized  $p_T$  distribution of jets (quarks, anti-quarks, and gluons) obtained by using CTEQ5L parton distribution function and EKS98 nuclear modification factor is given by:

$$\frac{dN^{\text{jet}}}{d^2p_T dy} \Big|_{y=0} = T_{AA} \frac{d\sigma^{\text{jet}}}{d^2p_T dy} \Big|_{y=0} = K \frac{a}{(1 + p_T/b)^c} \quad (37)$$

Here  $T_{AA} = 9A^2/8\pi R_\perp^2$  is the nuclear thickness for a head-on collision and to include the higher order effects a  $K$  factor of 2.5 is introduced. Numerical values for the parameters for quarks, anti-quarks and gluons can be found in the Ref. [9].

Now as a first step, let us ignore the transverse expansion of the plasma and assume that a thermally and chemically equilibrated plasma is produced in the collision at an initial time  $\tau_0$  at temperature  $T_0$ . In an isentropic longitudinal

expansion,  $T_0$  and  $\tau_0$  are related by the observed particle rapidity density ( $dN/dy$ ) by:

$$T_0^3 \tau_0 = \frac{2\pi^4}{45\zeta(3)} \frac{1}{4a\pi R_\perp^2} \frac{dN}{dy} \quad (38)$$

where  $a = 42.25\pi^2/90$ , for QGP consisting of  $u, d$  and  $s$  quarks and gluons.  $dN/dy$  can be taken as  $\simeq 1260$ , based on the charge particle pseudo-rapidity density measured by PHOBOS experiment [53] for central collision of  $Au$  nuclei at  $\sqrt{s_{NN}} = 200$  GeV. For central collision of  $Pb$  nuclei at LHC energies  $dN/dy \simeq 5625$  was used by Fries *et al.* [9] as in Ref. [54].

Further assuming a rapid thermalization, initial conditions can then be estimated as [54]  $T_0 = 446$  MeV and  $\tau_0 = 0.147$  fm/c for the RHIC and  $T_0 = 897$  MeV and  $\tau_0 = 0.073$  fm/c for the LHC. Now, taking the nuclei to be uniform spheres, the transverse profile for initial temperature is given by  $T(r) = T_0[2(1 - r^2/R_\perp^2)]^{1/4}$  where  $R_\perp = 1.2A^{1/3}$  fm. The same profile  $R(r) = 2(1 - r^2/R_\perp^2)$  is used for the jet production.

The jet traverses the QGP medium until it reaches the surface or until the temperature drops to the transition temperature  $T_c$  ( $\sim 160$  MeV).

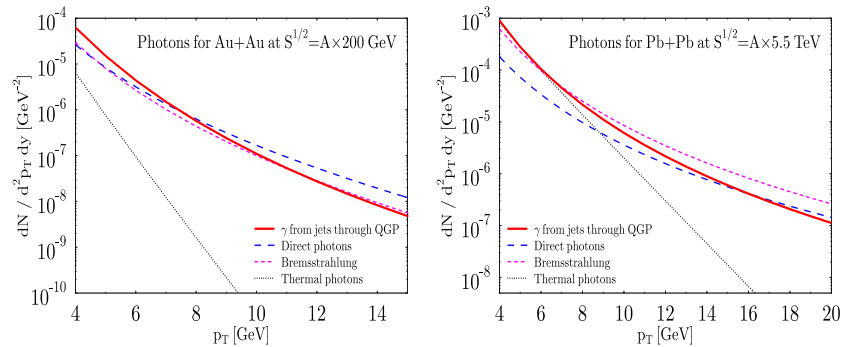


**Fig. 15.** Jet conversion photons at RHIC [left panel] and LHC [right panel] energies (taken from Ref. [9]).

First estimates for the jet conversion photons at RHIC and LHC energies along with other sources of photons having large transverse momentum are given in Fig. 15. We see that the jet conversion photons make a fairly large contribution in the  $p_T$  range of 4-10 GeV.

The centrality dependence of jet conversion photons was also studied by Fries *et al.* [55] (see figure 16), which indicates a small but clear contribution of photons due to passages of jets through the plasma. These early calculations have been brought to a high degree of sophistication by the McGill group [56] (see figure 17), where jet quenching and jet-photon conversion along with

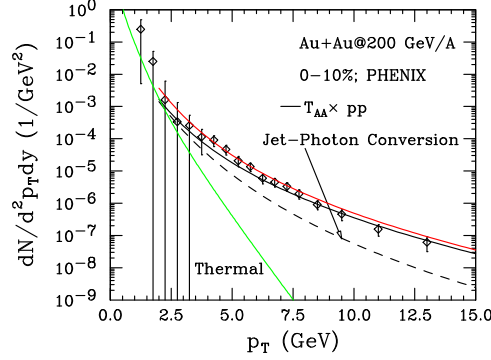


**Fig. 16.** Photon yield as a function of  $p_T$  in central (0-10%)  $Au + Au$  collisions at 200A GeV. Results of jet-photon conversion (solid and labeled), primary hard photons (dashed) and the sum of the two (upper-most solid curve) along with thermal photons are shown separately. Data are from the PHENIX collaboration [25].

bremsstrahlung is treated in a single frame work. The details can be seen in Ref. [56].

In Fig.17 the results for thermal photons, direct photons due to primary processes, bremsstrahlung photons and the photons coming from jets passing through the QGP in central collision of gold nuclei at RHIC energies is plotted. The quark jets passing through the QGP give rise to a large yield of high-energy photons. For RHIC this contribution is dominant source of photons up to  $p_T \simeq 6$  GeV. Due to multiple scattering suffered by the fragmenting partons a suppression of the bremsstrahlung contribution is found. This will further enhance the importance of the jet-photon conversion process.

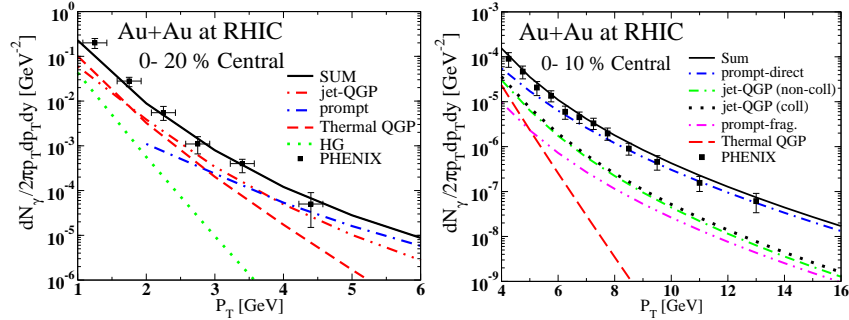


**Fig. 17.** Yield of photons in  $Au + Au$  collisions at RHIC, for centrality classes 0 – 10% (left panel) and 0 – 10% (right panel). See [56] for details. The data sets are from Refs. [57] and [25] respectively.



Obviously a high statistics data at several centralities and energies will go a long way in clearly establishing the presence of jet-conversion photons at RHIC and LHC energies. This is also of importance, as there are indications that these photons measure the initial spatial anisotropy of the system [56].

## 4 Dileptons

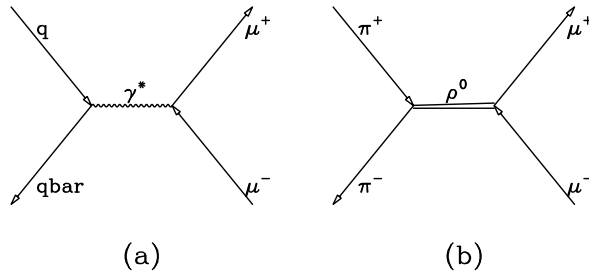


**Fig. 18.** Dilepton production from (a) quark anti-quark annihilation and (b)  $\pi^+\pi^-$  annihilation through  $\rho$  channel.

Virtual photons or dileptons are also very powerful and efficient probes like the real photons, to study the dynamics of heavy ion collisions and the properties of the medium created in the collisions. Real photons are massless, whereas dileptons are massive. Thus, invariant mass  $M$  and the transverse momentum  $p_T$  are the two parameters available for dileptons, which can be tuned to investigate the different stages of the expanding fireball. Dileptons having large invariant mass and high  $p_T$ , are emitted very early, soon after the collision when the temperature of the system is very high. On the other hand, those having lower invariant masses come out later from a relatively cooler stages and at low temperatures.

Similar to the real photons, dileptons are also emitted from every stage of heavy ion collisions [2]. In the QGP phase, a quark can interact with an anti-quark to form a virtual photon  $\gamma^*$ , which subsequently decays in to a lepton ( $l^-$ ) and an anti-lepton ( $l^+$ ) pair, together known as dilepton. In the hadronic phase, dileptons are produced from interactions of charged hadrons with their anti-particles by processes like  $(\pi^+ + \pi^- \rightarrow l^+ + l^-)$  (see Fig. 18). They are also produced from decay of hadronic resonances like  $\rho$ ,  $\omega$ ,  $\phi$ , and  $J/\Psi$  as well as from Drell-Yan process. In the Drell-Yan process, a valence quark from a nucleon in the projectile nucleus interacts with a sea anti-quark from a nucleon in the target nucleus to form a virtual photon, which decays into a lepton pair. The dilepton emissions can be classified into three distinct regimes in a rough estimation, depending on the invariant mass  $M$  of the emitted lepton pairs. These are:

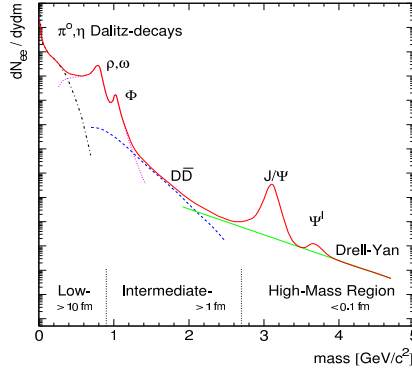


**Fig. 19.** Expected sources of dilepton production as a function of invariant mass in relativistic heavy ion collisions (schematic).

a) Low Mass Region (LMR):  $M \leq M_\phi (= 1.024 \text{ MeV})$ : In this mass range, vector meson decays are the dominating source of dilepton production and medium modified spectral density is one of the key issues which needs to be addressed.

b) Intermediate Mass Region (IMR):  $M_\phi < M < M_{J/\psi} (= 3.1 \text{ GeV})$ : In intermediate mass region, continuum radiation from QGP dominates the dilepton mass spectrum and thus this region is important for getting a pure QGP signature.

c) High Mass Region (HMR):  $M \geq M_{J/\psi}$ : In the HMR, the most interesting phenomenon are the primordial emission and heavy quarkonia like  $J/\psi$  and  $\Upsilon$  suppression.

A schematic diagram of continuous dilepton mass spectrum is shown in Fig. 19.

#### 4.1 Dileptons from QGP and hadronic phase

Dilepton production by quark anti-quark annihilation process or by  $\pi^+ \pi^-$  annihilation process can be expressed in a general form as,

$$a^+ + a^- \rightarrow l^+ + l^- \quad (39)$$

where, the particle ‘a’ can be either a quark or a  $\pi$  meson. We closely follow the treatment of Ref. [10] for calculation of dilepton spectra in this section. From Quantum Electrodynamics (QED), the cross section for  $e^+e^- \rightarrow \mu^+\mu^-$  can be written as,

$$\tilde{\sigma}(M) = \frac{4\pi}{3} \frac{\alpha^2}{M^2} \left[ 1 + \frac{2m_l^2}{M^2} \right] \left[ 1 - \frac{4m_l^2}{M^2} \right]^{1/2} \quad (40)$$

In the above equation,  $\alpha$  is the fine structure constant ( $\approx 1/137$ ),  $m_l$  is the mass of  $\mu$ , and  $M$  is the dilepton invariant mass. For the quark anti-quark annihilation process, this cross-section is modified by inclusion of a colour factor  $N_c (= 3)$ , and the fractional charges of the up(u) and down(d) quarks. Thus, the new cross-section takes the form as,

$$\sigma_q(M) = F_q \tilde{\sigma}(M), \quad (41)$$

$$F_q = N_c (2s + 1)^2 \sum_f e_f^2 \quad (42)$$

where  $s$  is the spin of quarks,  $e_f$  is the fractional charge, and the sum is over different quark flavour 'f'. If we consider only u and d quarks having fractional charges 1/3 and 2/3 respectively, then the factor  $F_q$  is 20/3.

In the hadronic phase, the  $\pi^+ \pi^-$  annihilation from vector meson dominance model can be expressed as,

$$\pi^+ + \pi^- \rightarrow \rho \rightarrow l^+ + l^- \quad (43)$$

For this case, the QED cross-section is multiplied by form factor  $F_\pi(M)$  which is of Breit-Wigner form as;

$$F_\pi(M) = \frac{m_\rho^4}{(m_\rho^2 - M^2)^2 + m_\rho^2 \Gamma_\rho^2} \quad (44)$$

Here,  $M_\rho$  is the mass of the  $\rho$  meson ( $\sim 770$  MeV) and  $\Gamma_\rho$  ( $\sim 155$  MeV) is the decay width. Thus, the total pion cross-section as a function of  $M$  becomes,

$$\sigma_\pi(M) = F_\pi \tilde{\sigma}(M) (1 - 4m_\pi^2/M^2)^{1/2}, \quad (45)$$

The reaction rate 'R' can be obtained from the kinetic theory:

$$R(a^+ a^- \rightarrow l^+ l^-) = \int \frac{d^3 p_1}{(2\pi)^3} f(\mathbf{p}_1) \int \frac{d^3 p_2}{(2\pi)^3} f(\mathbf{p}_2) \sigma(a^+ a^- \rightarrow l^+ l^-; \mathbf{p}_1 \mathbf{p}_2) v_{rel} \quad (46)$$

where,

$$v_{rel} = \frac{[(p_1 \cdot p_2)^2 - m_a^4]^{1/2}}{E_1 E_2} \quad (47)$$

$f(\mathbf{p})$ , is the occupation probability at momentum  $\mathbf{p}$  and energy  $E = \sqrt{\mathbf{p}^2 + m_a^2}$ . Now, using the distribution function  $f(\mathbf{p}) \sim e^{-E/T}$ , and integrating over five out of the six variables, the reaction rate takes a simplified form as,

$$R(T) = \frac{T^6}{(2\pi)^4} \int_{z_0}^{\infty} \sigma(z) z^2 (z^2 - 4z_a^2) K_1(z) dz \quad (48)$$

Here,  $z = M/T$ ,  $z_a = m_a/T$ , and  $K_1$  is the modified Bessel function of the first kind. The value of the parameter  $z_0$  is taken as the larger of  $2m_a/T$

and  $2m_l/T$ . Now, for massless  $u$  and  $d$  quarks ( as  $m_u, m_d \ll T$ ), the  $e^+e^-$  emission rate takes a simple form of  $T^4$  law,

$$R = \frac{10}{9\pi^3} \alpha^2 T^4. \quad (49)$$

One can also estimate the relaxation time for lepton pairs to come to equilibrium with the QGP:

$$t_{\text{rel}} = \frac{n_{\text{eq}}^l}{2R} = \frac{9\pi}{10\alpha^2 T}. \quad (50)$$

For a temperature range of 200 to 500 MeV, the value of  $t_{\text{rel}}$  varies from  $20 - 60 \times 10^3$  fm/ $c$ . We know that the life time of the QGP phase is only  $\sim 10$  fm/ $c$ , which is more than three order of magnitude smaller than  $t_{\text{rel}}$ . Thus, like the real photons, the produced lepton pairs also escape the system without suffering significant absorption in the medium.

Now, the dilepton emission rate  $R$  is actually defined as the total number of lepton pairs emitted from a 4-volume element  $d^4x$  ( $= d^2x_T d\eta \tau d\tau$ ) at a particular temperature  $T$  is given by:

$$R = dN/d^4x. \quad (51)$$

Thus, the rate of production of dileptons having invariant mass  $M$  can be expressed using Eqn.(46) as,

$$\frac{dN}{d^4x dM^2} = \frac{\sigma(M)}{2(2\pi)^4} M^3 T K_1(M/T) \left[ 1 - \frac{4m_a^2}{M^2} \right]. \quad (52)$$

From the last equation and using properties of the modified Bessel's functions, the production rate per unit 4-volume for total energy  $E$ , momentum  $p$  and invariant mass  $M$  (where,  $E = \sqrt{p^2 + M^2}$ ) can be written as,

$$E \frac{dN}{d^4x dM^2 d^3p} = \frac{\sigma(M)}{4(2\pi)^5} M^2 e^{-E/T} \left[ 1 - \frac{4m_a^2}{M^2} \right]. \quad (53)$$

Integrating the rate of emission over the entire 4-volume from QGP and hadronic phase, one can obtain the  $p_T$  spectra at a particular  $M$  as,

$$\begin{aligned} \frac{dN}{dM^2 d^2p_T dy} = & \int \tau d\tau r dr d\eta d\phi \left[ \left[ E \frac{dR}{dM^2 d^3p} \right]_{\text{QGP}} f_{\text{QGP}}(r, \tau) \right. \\ & \left. + \left[ E \frac{dR}{dM^2 d^3p} \right]_{\text{HM}} f_{\text{HM}}(r, \tau) \right] \end{aligned} \quad (54)$$

where,  $\eta$  is the space time rapidity. In the above equation, the temperature  $T$ , QGP and hadronic matter (HM) distribution functions ( $f_{\text{QGP}}, f_{\text{HM}}$ ), all are functions of space  $\mathbf{r}$  ( $x, y$ ), transverse velocity  $v_T$ , and proper time  $\tau$ . Eqn. (54) can be solved numerically by using any appropriate model [e.g., Ref. [58]] with a proper equation of state (EOS). One can also get the invariant mass spectrum by integrating out the variable  $p_T$  from Eqn. (54). The invariant mass spectrum of thermal dilepton is dominated by QGP radiation above  $\phi$  mass and hadronic radiation outshines the QGP contribution for  $M \leq M_\phi$ .

## 4.2 Medium modification

As mentioned earlier, in the low mass region, dilepton emission is largely mediated by  $\rho(770)$ , a broad vector meson, as a result of its strong coupling to the  $\pi\pi$  channel and a short lifetime, which is about  $1.3 \text{ fm}/c$ . In-medium properties of vector mesons, like change in medium mass and width have long been considered as prime signatures of a hot and dense hadronic medium. CERES/NA45 [59, 60] started the pioneering experiment on dilepton measurement during the period 1989-1992 at CERN SPS. For  $p + Be$  and  $p + Au$  collisions, the theoretical estimates, considering only hadron decay (as source of dilepton production), were in excellent agreement with the experimental data points. However, the CERES/NA45 experimental data for  $S + Au$  and  $Pb + Au$  at  $200A \text{ GeV}$  and  $158A \text{ GeV}$  respectively exhibit excess radiation beyond the electromagnetic final state decay of produced hadrons below the  $\phi$  mass. From these observations, it was concluded that, the theoretical models based on  $\pi\pi$  annihilation can reproduce the experimental data, only if the properties of the intermediate  $\rho$  meson is modified in the medium. This was an exciting discovery and a genuine consequence of many body physics. However, the resolution and statistical accuracy of the data was insufficient to distinguish between models suggesting a drop in the mass of  $\rho$  mesons [61] and those which suggest an increase in their decay width [62] and thus, determine the in-medium spectral properties of the  $\rho$  meson.

Shortly after this, an excess dimuon (over the sources expected from  $pA$  measurement) was identified experimentally by Helios/3 [63] (measured both  $e^+e^-$  and  $\mu^+\mu^-$ ) and NA38/NA50 [64] collaborations.

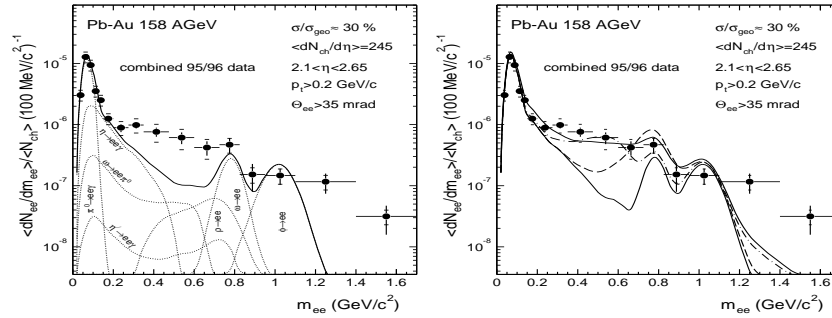


**Fig. 20.** Left panel: Invariant mass spectrum of  $e^+e^-$  pairs emitted in  $158A \text{ GeV}$   $Pb + Au$  collisions from the combined analysis of 1995 and 1996 data by CERES/NA45 [59, 60]. The solid line shows expected yield from hadron decay and dashed lines indicate the individual contribution to the total yield. Right panel: Comparison of the experimental data to i) free hadron decays without  $\rho$  decays (thin solid line), ii) model calculations with a vacuum  $\rho$  spectral function (thick dashed line), iii) with dropping in-medium  $\rho$  mass (thick dash-dotted line), iv) with a medium modified  $\rho$  spectral function (thick solid line).

Rapp and Shuryak [65] and Kvasnikova *et al.* [48] showed that, the excess dimuon observed by NA50 in the mass region  $1.5 < M < 2.5$  GeV can be explained by thermal signal without invoking any anomalous enhancement in the charm production. Kvasnikova *et al.* studied the NA50 intermediate mass dimuon result using hydrodynamic model and a detailed analysis of the rates of dilepton production from hadronic phase [48]. Detector resolution and acceptance were accurately modeled in their calculation and the normalization was determined by a fit to the Drell-Yan data using the MRSA parton distribution function as done in the experimental NA50 analysis. The results are shown in Fig. 21. They also studied the centrality dependence of the NA50 data using hydrodynamics by incorporating azimuthal anisotropy in the calculation. The results were in fairly good agreement with the measured excess dilepton data, as can be seen in the third panel of Fig. 21.

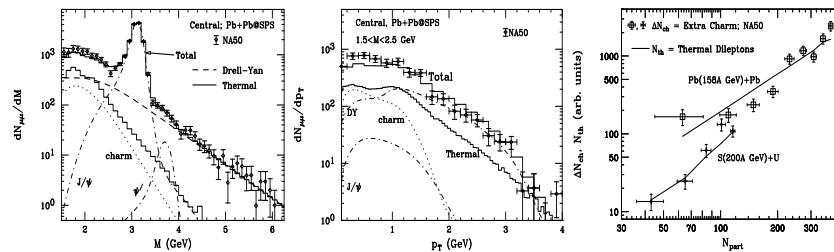


**Fig. 21.** (a) The dimuon invariant mass spectrum after correcting for detector acceptance and resolution and NA50 data. The Drell-Yan and thermal contributions are shown separately along with correlated charm decay and direct decays of the  $J/\psi$  and  $\bar{J}/\psi$ . (b) The dimuon transverse momentum spectrum. (c) Centrality dependent results from Ref. [48] and NA50 data [64].

### Dropping $m_\rho$ vs. increasing $\Gamma_\rho$

The CERES data [59, 60] was unable to distinguish between the models suggesting drop in the mass of  $\rho$  meson and those suggesting an increase in its width, as seen in Fig. 20. The high statistics data obtained by the NA60 Collaboration for  $In + In$  collisions at SPS energies for the dimuon excess rather clearly ruled out the models advocating the dropping mass scenarios. They rather firmly establish the models advocating the substantial broadening of the decay width of the  $\rho$  meson due to many body effects (see Fig 22).

## 5 Elliptic Flow

Elliptic flow is one of the key observables in relativistic collisions of heavy nuclei, which confirms the collectivity and early thermalization in the created hot

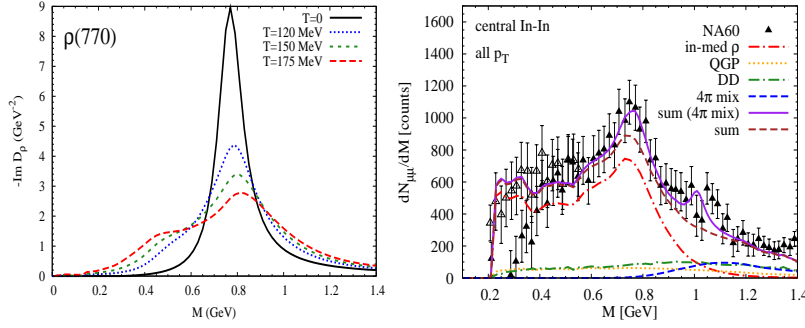


**Fig. 22.** Left panel: In medium vector meson spectral functions from hadronic many body theory. The  $\rho$  in cold nuclear matter at several densities proportional to the saturation density  $\rho_0 = 0.16 \text{ fm}^{-3}$ . Right panel: NA60 [66] excess dimuons in central  $In + In$  collisions at SPS compared to thermal dimuon radiation using in-medium electromagnetic rates [67].

and dense matter. For a non-central collision (impact parameter  $b \neq 0$ ) of two spherical nuclei, the overlapping zone between the nuclei no longer remains circular in shape, rather it takes an almond shape. This initial spatial anisotropy of the overlapping zone is converted into momentum space anisotropy of particle distribution via the action of azimuthally anisotropic pressure gradient, which gives rise to elliptic flow [68]. Note that, this anisotropic flow or elliptic flow can also be produced in central collisions of deformed nuclei, such as  $U + U$  collisions [69]. The driving force for momentum anisotropy is the initial spatial eccentricity  $\epsilon_x (= \langle y^2 - x^2 \rangle / \langle y^2 + x^2 \rangle)$  and the momentum anisotropy can grow as long as  $\epsilon_x > 0$  [70]. Elliptic flow coefficient  $v_2$  is quantified as the second Fourier co-efficient of particle distribution in the  $p_T$  space, which is of the form:

$$\frac{dN(b)}{p_T dp_T dy d\phi} = \frac{dN(b)}{2\pi p_T dp_T dy} (b) \times [1 + 2v_1(p_T, b) \cos(\phi) + 2v_2(p_T, b) \cos(2\phi) + 2v_3(p_T, b) \cos(3\phi) + \dots]. \quad (55)$$

At mid-rapidity ( $y = 0$ ) and for collisions of identical nuclei, only the even cosine terms survive in the above Fourier series and  $v_2$  is the lowest non-vanishing anisotropic flow co-efficient. Now, the value of  $v_2$  depends on the impact parameter  $b$ , transverse momentum  $p_T$  as well as on the particle species through their rest masses  $m$ . For massless real photons,  $v_2$  depends on the elliptic flow of parent particles.

### 5.1 Thermal Photon $v_2$

Elliptic flow co-efficient  $v_2$  for photons is a much more powerful tool than the  $v_2$  of hadrons, to study the evolution history of the system depending on the

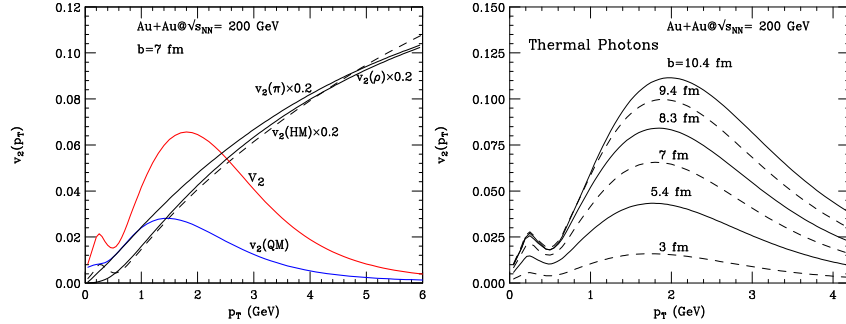


**Fig. 23.** Left panel:  $v_2(p_T)$  for thermal photons along with the  $v_2$  for  $\pi$  and  $\rho$  mesons. Contributions from the quark matter and the hadronic matter are shown separately with the sum contribution. Right panel: Thermal photon  $v_2$  for different centrality bins [taken from Ref. [7]].

different emission time and production mechanism of photons compared to hadrons. Photons are emitted from all stages and throughout the evolution of the system, whereas, hadrons are emitted only from the freeze-out surface at a relatively much cooler temperature ( $\sim 100$  MeV). The interplay of the photon contributions from fluid elements at different temperatures with varying radial flow pattern, gives the photon  $v_2$  a richness, which is not possible for hadrons. Also, photons emitted from QGP phase as a result of  $q\bar{q}$  annihilation and quark gluon Compton scattering, carry the momenta of the parent quarks or anti-quarks, which makes them an unique tool for QGP study.

Ideal hydrodynamic model has successfully predicted the elliptic flow for different hadronic species upto a  $p_T$  value of 1.5(2.3) GeV for mesons (baryons) [70] at RHIC. Experimental data show that,  $v_2(p_T)$  for hadrons saturates beyond that  $p_T$  range. However, ideal hydrodynamics predicted  $v_2(p_T)$  rises monotonically with  $p_T$ . The saturation at higher  $p_T$  is often explained as due to viscosity, neglected in the discussion here.

Fig. 23 shows the  $p_T$  dependent  $v_2$  for thermal photons [7] for a typical impact parameter  $b = 7$  fm. Contributions from quark matter (QM) and hadronic matter (HM) along with the sum of the two are shown separately (left panel of Fig. 23). One can see that,  $v_2(HM)$  rises monotonically with  $p_T$ , similar to the hadronic  $v_2$  predicted by hydrodynamics. On the other hand,  $v_2(QM)$  is very small at high  $p_T$  or early times, as very little flow is generated by that time.  $v_2(QM)$  rises for smaller values of  $p_T$  and after attaining a peak value around 1.5 – 2.0 GeV, it tends to 0 as  $p_T \rightarrow 0$ . The total flow or  $v_2(QM+HM)$  tracks the  $v_2(QM)$  at high  $p_T$  in spite of very large  $v_2(HM)$ , as the yield of photons from hadronic phase is very small at high  $p_T$ . It is well known and mentioned earlier that, for photon energy larger than the rest masses of the photon emitting particles, the photon production cross-section peaks when the photon momentum and momentum of photon emitting particles become almost identical [2]. Thus, at high  $p_T$  photon  $v_2$



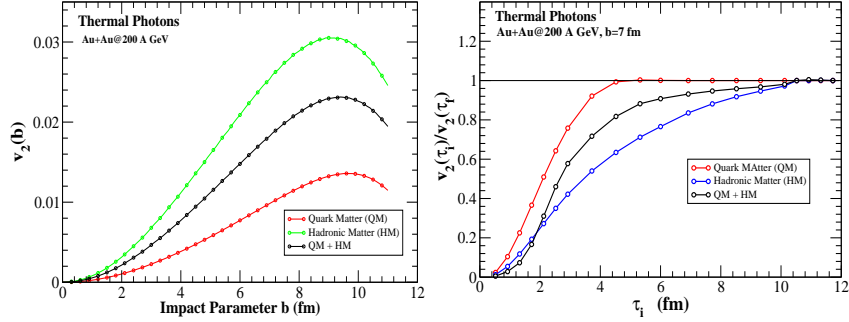


**Fig. 24.** Left panel:  $p_T$  integrated elliptic flow of thermal photons from different phases at RHIC. Right panel: Time evolution of elliptic flow from different phases, normalized by the final value at the time of freeze-out [taken from Ref. [71]].

reflects the anisotropies of the quarks and anti-quarks at early times. Also, the collision induced conversion of vector mesons ( $\rho$ ) starts dominating the photon production for  $p_T \geq 0.4$  GeV, which gives rise to a structure at the transition point in the photon  $v_2$  curve [7]. As HM contribution dominates the  $p_T$  spectrum and hydrodynamics is well applicable around that  $p_T$  range, the structure is expected to survive in the experimental result also.

Recently Turbide *et al.* [56] have shown that, total contribution to photon  $v_2$  from prompt fragmentation (small  $+ve v_2$ ) and jets-conversion (small  $-ve v_2$ ) photons is very small, almost equal to zero. Also, we know that the prompt photons from Compton and annihilation processes do not contribute to elliptic flow as their emission is not subjected to collectivity and has azimuthal symmetry. Thus, at low and intermediate  $p_T$  range,  $v_2$  from thermal photons plays a dominant role in deciding the nature of the direct photon  $v_2$ .

For central collision of two spherical nuclei, the spatial eccentricity ( $\epsilon$ ) of the overlapping zone is zero, thus the flow co-efficient  $v_2$  is also zero. The  $v_2(p_T)$  for thermal photons for different centrality bins are shown in the right panel of Fig. 23, where the value of  $v_2$  rises from central towards peripheral collisions. Now, the elliptic flow as well as spatial eccentricity both rise with higher values of impact parameter. However, the ratio of the two remains independent of impact parameter up to a very large value of  $b$  [71]. The  $p_T$  integrated  $v_2$  for thermal photons from different phases as a function of collision centrality shows an interesting behavior (left panel of Fig. 24). The  $v_2(b)$  rises with  $b$  until for very peripheral collisions. For these the system size itself becomes very small to generate enough pressure gradient and elliptic flow, and as a result  $v_2(b)$  decreases. The  $p_T$  dependent as well as  $p_T$  integrated time evolution results [71] of thermal photon spectra and elliptic flow show explicitly the gradual build up of spectra and  $v_2$  with time very well. The photon  $v_2$  from QGP phase saturates within about 4-5 fm/c (right panel of

Fig.24), whereas  $v_2$  from hadronic phase is not very significant at early times and it saturates much later.

## 5.2 Thermal Dilepton $v_2$

Elliptic flow of thermal dileptons is another very interesting and illustrative observable which gives information of the different stages of heavy ion collision depending on invariant mass  $M$  and transverse momentum  $p_T$  [72]. At the  $\rho$  and  $\phi$  masses, the  $p_T$  spectra and  $v_2(p_T)$  show complete dominance of hadronic phase. At these resonance masses radiation from quark matter becomes significant only for very large  $p_T (\geq 4)$  GeV (left panel of Fig. 25). The  $v_2(p_T)$  at  $M = m_\rho$  also shows similar nature as spectra and the total  $v_2$  is almost similar to hadronic  $v_2$  upto a large  $p_T$ . Right panel of Fig. 25 shows dilepton  $v_2$  at rho mass along with  $v_2$  of rho meson where,  $v_2(HM)$  tracks  $v_2(\rho)$ . Also, the hadronic  $v_2$  is little smaller than the  $v_2(HM)$  for dileptons. The effective temperature of dilepton emission is a little larger than for hadrons, thus the spectra of the later is boosted by a somewhat larger radial flow [72], which results in smaller elliptic flow.

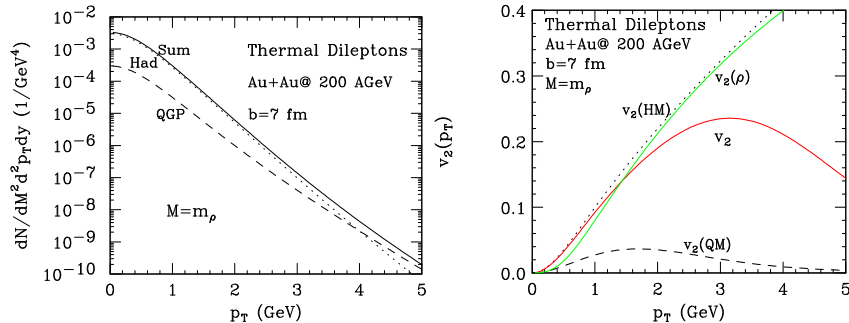


**Fig. 25.**  $p_T$  spectra [left panel] and  $v_2$  [right panel] for thermal dileptons at  $M = m_\rho$ .  $v_2(\rho)$  is also plotted in the  $v_2$  curve for comparison [72].

A totally different situation emerges for the  $p_T$  spectrum and  $v_2$  for dilepton invariant mass  $M > M_\phi$ . For  $M = 2$  GeV, the dilepton  $v_2$  is similar to  $v_2(QM)$  in spite of the 20 times larger  $v_2(HM)$ , as hadronic dileptons are very few compared to QGP radiation at this  $M$  value (Fig. 26).

The  $p_T$  integrated spectra and  $v_2$  as a function of invariant mass  $M$  show well defined peaks at the resonance masses ( $\rho$ ,  $\omega$  and  $\phi$ ), as can be seen Fig. 27. For  $M \leq M_\phi$  the dilepton spectrum is totally dominated by hadronic phase and above that it is dominated by contribution from QGP.  $v_2(QM)$  is very small at large  $M$  and rises for smaller  $M$ . It shows a nature similar to the thermal photon  $v_2$ . The  $M$  dependent  $v_2(HM)$  is significant only at the resonance masses and beyond  $\phi$  mass its contribution to total  $v_2$  is negligible.

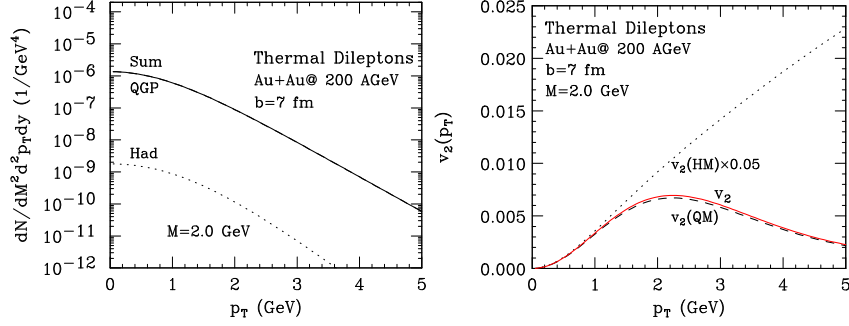


**Fig. 26.**  $p_T$  spectra [left panel] and  $v_2$  [right panel] for thermal dileptons at  $M = 2$  GeV [72].

Thus, for large values of  $M$  or at early times flow comes from QGP phase and its value is very small, whereas at later times or at low  $M$  values it is from HM, which is very strong. The measurement of flow parameter at high  $M$  and/or high  $p_T$  values can be very useful to reveal a pure QGP signature.

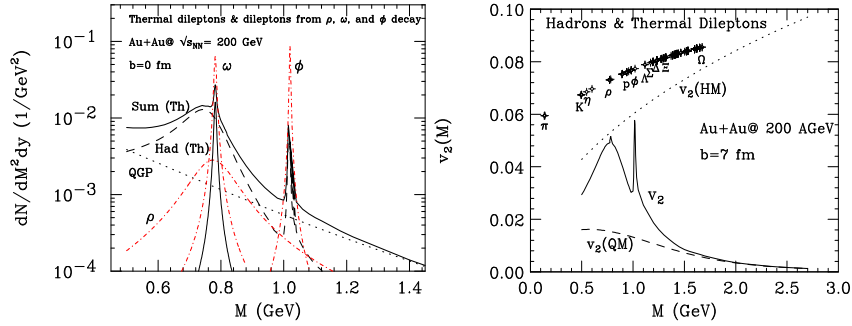


**Fig. 27.** Left panel: The mass spectra of thermal dileptons from a hydrodynamical simulation of central 200A GeV  $Au + Au$  collision. Quark and hadronic matter contributions are shown separately. Right panel:  $p_T$  integrated elliptic flow parameter for dileptons and various hadrons [72].

### 5.3 Elliptic flow of decay photons

We have already discussed that most of the produced photons in heavy ion collisions are from the  $2\text{-}\gamma$  decay of  $\pi^0$  and  $\eta$  mesons and the direct photons contain a small fraction of the inclusive photon spectrum. Thus it is very interesting to know the nature of  $v_2$  of decay photons from pion and  $\eta$  decays. The momentum distribution of decay photons from  $\pi^0$  decay in an invariant form can be expressed as [73],

$$k_0 \frac{dN}{d^3k}(p, k) = \frac{1}{\pi} \delta(p \cdot k - \frac{1}{2}m^2), \quad (56)$$

where  $p$  and  $k$  are the 4-momentum of the pion and photons and  $m$  is the pion

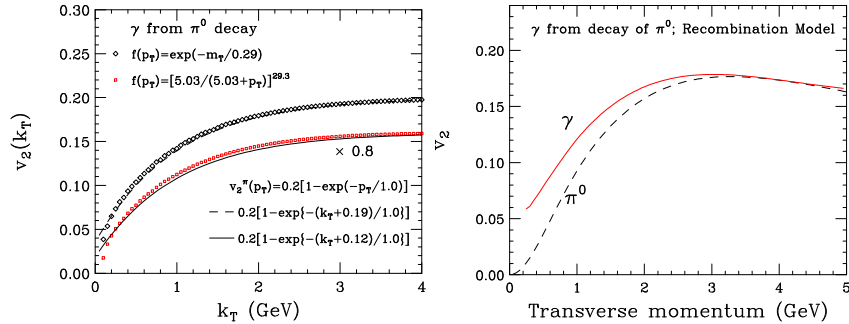


**Fig. 28.** Left panel: Elliptic flow of photons from  $\pi^0$  decay at mid-rapidity.  $f(p_T)$  stands for the momentum distribution of the  $\pi^0$ . Right panel: Elliptic flow parameters for photons from decay of  $\pi^0$  obtained using the recombination model [taken from Ref. [74]].

mass. Thus the Lorentz invariant cross-section of the decay photons using the decay kinematics from the Eqn. (56) is,

$$k_0 \frac{d\sigma}{d^3k} = \int \frac{d^3p}{E} \left( E \frac{d\sigma}{d^3p} \right) \frac{1}{\pi} \delta(p \cdot k - \frac{1}{2}m^2). \quad (57)$$

Layek *et al.* [74] have calculated elliptic flow of decay photons considering several azimuthally asymmetric pion distributions (Fig. 28). They have shown that  $k_T$  dependent  $v_2$  of decay photons closely follows the  $v_2(p_T)$  of  $\pi^0$  evaluated at  $p_T \sim k_T + \delta$  (where  $\delta \sim 0.1 - 0.2$  GeV). Similar results were obtained for decay photons from  $\eta$  mesons also. This study could be useful in identifying additional sources of photons as the  $v_2$  of  $\pi^0$  is similar to that of  $\pi^+$  and  $\pi^-$ . Also by using the property of quark number scaling or the recombination model, the decay photon  $v_2$  can help to estimate the  $v_2$  of constituent partons in the  $\pi^0$  or  $\eta$  mesons (right panel of Fig. 28). See Ref. [74] for details.

### Experimental measurement of direct photon $v_2$

PHENIX has measured direct photons and its  $v_2$  by subtracting  $v_2$  of decay photons (2- $\gamma$  decay of  $\pi^0$  and  $\eta$  mesons) from inclusive photon  $v_2$  using appropriate weight factor [75]. The procedure followed by them to estimate direct photon  $v_2$  is as follows:

$$v_2^{\text{dir.}} = \frac{R \times v_2^{\text{incl.}} - v_2^{\text{bkgd.}}}{R - 1} \quad (58)$$

where  $R$  is the direct photon excess over hadron decays defined as,

$$R = \frac{(\gamma/\pi^0)_{\text{incl.}}}{(\gamma/\pi^0)_{\text{bgd.}}} \quad (59)$$

The factor  $R$  is measured from spectral analysis. The inclusive and hadron

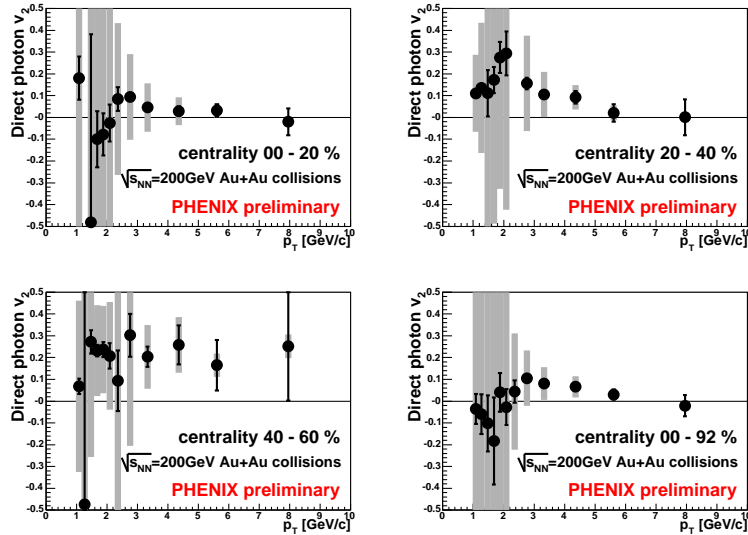


**Fig. 29.** Elliptic Flow of direct photons from 200A GeV  $Au + Au$  collision at RHIC [76].

decay  $v_2$  are measured using reaction plane method where the background photons are measured using a Monte Carlo simulation. We have already seen that the photon  $v_2$  shows different signs and/or magnitude depending on the production procedure of photons in heavy ion collisions. Thus experimental measurement of photon  $v_2$  can be a very powerful tool to disentangle the intermix contributions from different sources in different  $p_T$  ranges. However, the experimentally measured preliminary PHENIX data still contain a large systematic error (Fig. 29), which need to be reduced before making any specific conclusion about direct photon  $v_2$ .

## 6 Photon tagged jets

Jets are hard phenomenon characterized by a large momentum transfer between partons and are characterized by several hadrons in a small angle around

a leading particle as a result of jet fragmentation. The hadrons surrounding a jet are known as associated particles of the jet.

One of the key observables at RHIC energy is the strong suppression of leading hadron yield at high values of transverse momentum compared to expectations based on  $p + p$  or  $d + A$  collisions at same collision energy. This is the celebrated phenomenon of ‘jet quenching’. It is assumed that the hard partons lose a large fraction of their energy when passing through the strongly interacting medium. A variety of qualitatively different models are available using collisional energy loss and radiative energy loss mechanisms to describe the nuclear modification factor  $R_{AA}$ , defined as,

$$R_{AA}(p_T, y) = \frac{d^2 N_{AA}/dp_T dy}{T_{AA}(b) d^2 \sigma^{NN}/dp_T dy} \quad (60)$$

Here,  $T_{AA}$  is the nuclear overlap function and  $\sigma_{NN}$  is the nucleon-nucleon cross-section. The major problem for studying jet properties arises from the fact that, conventional calorimetric study can not measure the jet energy loss very accurately. Also it is very difficult to directly measure the modification of jet fragmentation function and jet production cross-section.

The ‘jet quenching’ in heavy ion collisions can be studied by measuring the  $p_T$  distributions of charged hadrons in opposite direction of a tagged direct photon. Quark-gluon Compton scattering and quark anti-quark annihilation process are the main mechanisms by which direct photons are produced at very high  $p_T$ , and jets are produced in the opposite direction of these photons. From momentum conservation law, the initial transverse energy of the produced jets are equal to that of the produced photons, i.e,  $E_\gamma = E_{\text{jet}}$ . Thus uncertainties regarding the jet cross-section can be avoided by tagging a direct photon in the direction opposite to the jet (see. Ref. [77]).

Medium modified parton fragmentation function  $D_{h/a}(z)$  ( $z$  is fractional momenta of the hadrons) is used to study the jet energy loss. The differential  $p_T$  distribution of hadrons from jet fragmentation in the kinematical region  $(\Delta\phi, \Delta y)$  using  $D_{h/a}(z)$  can be written as:

$$\frac{dN_{\text{ch}}^{\text{jet}}}{dy d^2 p_T} = \sum_{r,h} r_a(E_T^\gamma) \frac{D_{h/a}(p_T/E_T)}{p_T E_T} \frac{C(\Delta y \Delta\phi)}{\Delta y \Delta\phi}, \quad (61)$$

where,  $C(\Delta y \Delta\phi) = \int_{|y| \leq \Delta y/2} dy \int_{|\phi - \bar{\phi}_\gamma| \leq \Delta\phi/2} d\phi f(y - |\phi - \bar{\phi}_\gamma|)$  is an overall factor and  $f(y, \phi)$  is the hadron profile around the jet axis and  $r_a(E_T^\gamma)$  is the fractional production cross section of a typical jet associated with the direct photons. Thus, comparison between extracted fragmentation function in  $AA$  and  $pp$  collisions can be used to determine the jet energy loss as well as the interaction mean free path in the dense matter produced in high energy heavy ion collisions. Thorston Renk [78] has shown that by gamma hadron correlation measurement, the averaged probability distributions for quarks are accessible experimentally and he has also explained an analysis procedure

capable of distinguishing between different energy loss scenarios leading to the same nuclear suppression factor.

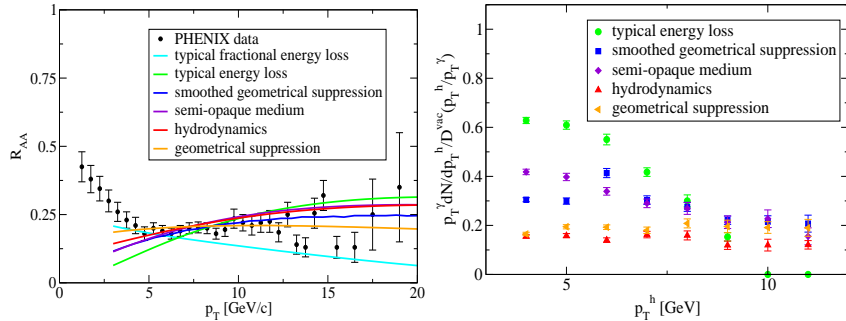


**Fig. 30.** Left panel: Nuclear suppression factor  $R_{AA}$  for different toy models and hydrodynamical simulation compared with PHENIX data. Right panel: Momentum spectrum of hard hadrons correlated back to back with a photon trigger normalized to the expectation of geometrical absorption (taken from Ref [78]).

### Isolating the bremsstrahlung photons

In order to measure direct photon cross section by suppressing the hadron decay background or in particular to isolate bremsstrahlung photons from accompanying hadrons, an interesting method known as ‘isolation cut’ can be used successfully. The basic assumption for performing the cut is that the hadronic energy in a cone around the photon is less than a certain fraction of the photon energy, i.e, a photon is considered as isolated if the combined energy of the accompanying hadrons is less than  $\epsilon E_\gamma$  ( where,  $E_\gamma$  is the photon energy) inside a cone of half opening angle  $\delta$  around the photon. The parameter  $\epsilon$  is very small ( $\sim 0.1$ ) and is called the energy resolution parameter. The cone around the tagged photon is known as isolation cone. The cone opening can be related to the radius  $R$  of a circle centered around the photon in the centre of mass system, where  $R$  is defined in terms of rapidity  $\eta$  and azimuthal angle  $\phi$  as,

$$R \geq \sqrt{\Delta\eta^2 + \Delta\phi^2} \quad (62)$$

For small rapidities, the half opening angle  $\delta$  equals the radius  $R$ . This method was successfully implemented into the theoretical study of isolated prompt photon production considering fragmentation contribution also in next-to-leading order (NLO) by Gordon and Vogelsang [21]. A very good accuracy of this method over a wide range of isolation parameters for prompt photon production was demonstrated in their calculation. Results from RHIC and LHC for this would be very valuable.

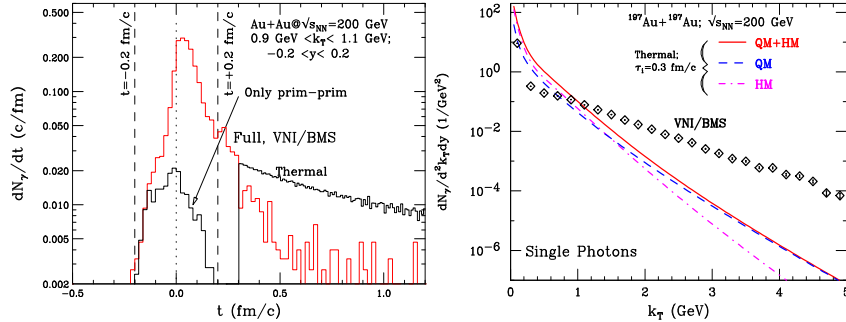


**Fig. 31.** Left panel: The production rate (per event) of hard photons in a central collision of gold nuclei at  $\sqrt{s_{NN}} = 200$  GeV as a function of time in the centre of mass system. Right panel: Spectrum of photons from various sources. QM and HM denote quark matter and hadronic matter contribution respectively (figures are from Ref. [6]).

### Dilepton tagged jets

In the study of photon tagged jets, the main problem arises from the jet pair production background, where a leading  $\pi^0$  in the jet is misidentified as a photon. For an event having a huge background ‘isolation cut’ is not a very efficient mechanism in the low  $p_T$  range to study photon tagged jets in heavy ion collisions and it is useful only for  $pp$  collisions. In the high  $p_T$  range although the background contribution related problems are reduced, a substantial problem in photon isolation is created by small opening angle. On the contrary jets tagged by dileptons are not affected by background and can be used to observe  $p_T$  imbalance, a signal of medium induced partonic energy loss. As we have mentioned earlier, for dileptons not only  $p_T$  but also invariant mass  $M$  is another equally important parameter which can be used accordingly to study dilepton tagged jets in the medium. At high  $p_T$  and high  $M$ , the dilepton yield is much lower compared to low  $p_T$  and low  $M$  range, however the relative background contribution is also lower in that range.

At very high transverse momentum Drell-Yan process ( $h_1 + h_2 \rightarrow l^+ l^- + X$ ) dominates the dilepton production from QGP phase. Srivastava *et al.* [79] have estimated the results for dilepton tagged jets by studying Drell-Yan process at NLO in relativistic heavy ion collisions at RHIC and LHC energies. They have also shown that correlated charm and bottom decay are unimportant as background for dileptons having large transverse momentum or in the kinematical region of interest for jet quenching. Lokhtin *et al.* [80] have studied the dimuon + jet production (including both  $\gamma^*/Z \rightarrow \mu^+ \mu^-$  modes) at LHC energy and have shown the  $p_T$  imbalance between  $\mu^+ \mu^-$  pair and a leading particle in a jet is clearly visible even for moderate energy loss. It is directly related to absolute value of partonic energy loss and almost insensitive to the angular spectrum of emitted gluons and to experimental jet energy resolution.



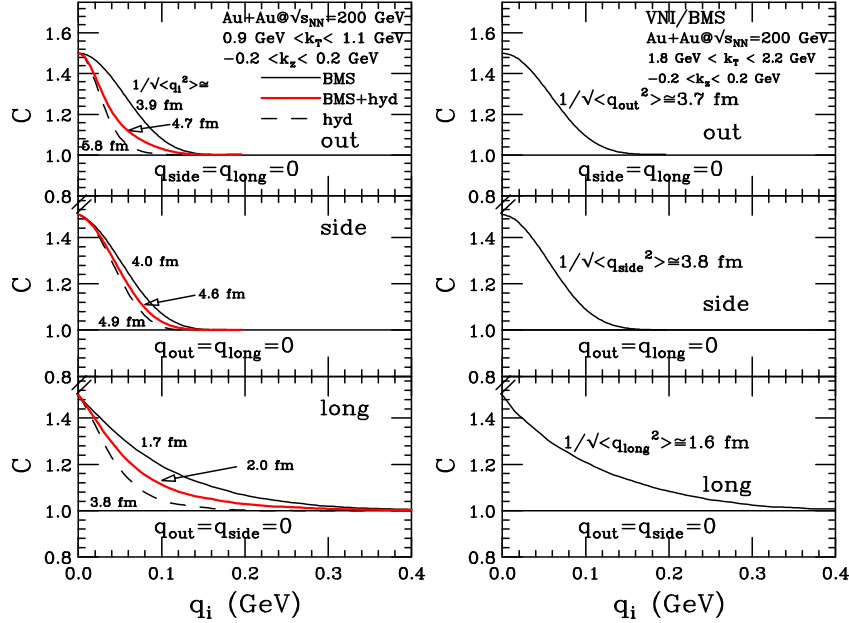


**Fig. 32.** Left panel: The outward, side-ward and longitudinal correlations of direct photon predicted by PCM at  $K_T = 2$  GeV, inclusion of thermal photons changes the results only marginally. Right panel: Intensity correlation of photons at 1 GeV, considering only PCM(BMS), only thermal (hyd), and all PCM+ thermal photons (BMS+hyd) (see Ref. [6]).

## 7 Intensity interferometry of thermal photons

The quantum statistical interference between identical particles emitted in relativistic heavy ion collisions, provide valuable insight about the shape and size of the particle emitting source. We know that direct photons emitted from different stages of the collision dominate the  $p_T$  spectra depending on the range of transverse momentum range. Thus, one can extract space time dimension of the system at different stages of the collision by measuring the correlation radii for photons at different transverse momentum.

Two particle correlation function  $C(\mathbf{q}, \mathbf{K})$  for photons having momenta  $\mathbf{k}_1$  and  $\mathbf{k}_2$ , emitted from a completely chaotic source can be written as,

$$C(\mathbf{q}, \mathbf{K}) = 1 + \frac{1}{2} \frac{|\int d^4x S(x, \mathbf{K}) e^{iq \cdot x}|^2}{\int d^4x S(x, \mathbf{k}_1) \int d^4x S(x, \mathbf{k}_2)} \quad (63)$$

In the above equation the factor 1/2 appears for averaging over spin and  $S(x, \mathbf{K})$  is the space time density function defined as,

$$E \frac{dN}{d^3K} = \int d^4x S(x, \mathbf{K}) \quad (64)$$

where,

$$\mathbf{q} = \mathbf{k}_1 - \mathbf{k}_2, \mathbf{K} = (\mathbf{k}_1 + \mathbf{k}_2)/2 \quad (65)$$

The correlation function  $C(\mathbf{q}, \mathbf{K})$  can be expressed in terms of outward, side-ward and longitudinal momentum difference and radii ( $q_{\text{out}}, q_{\text{side}}, q_{\text{long}}$  and  $R_{\text{out}}, R_{\text{side}}, R_{\text{long}}$  respectively) as,

$$C(q_{\text{out}}, q_{\text{side}}, q_{\text{long}}) \sim 1 + \frac{1}{2} \exp[-(q_{\text{out}}^2 R_{\text{out}}^2 + q_{\text{side}}^2 R_{\text{side}}^2 + q_{\text{long}}^2 R_{\text{long}}^2)/2] \quad (66)$$

Photon four momentum in terms of transverse momentum  $k_T$ , rapidity  $y$  and azimuthal angle  $\psi$  can be expressed as

$$k^\mu = (k_T \cosh y, k_T \cos \psi, k_T \sin \psi, k_T \sinh y) \quad (67)$$

and

$$\begin{aligned} q_{\text{long}} &= |k_{1z} - k_{2z}| = |k_{1T} \sinh y_1 - k_{2T} \sinh y_2| \\ q_{\text{out}} &= \mathbf{q}_T \cdot \mathbf{k}_T / k_T, \\ q_{\text{side}} &= |\mathbf{q}_T - q_{\text{out}} \mathbf{k}_T / k_T| \end{aligned}$$

Photon interferometry in the QGP phase has been investigated by several theoretical groups and the first experimental results on direct photon was obtained by WA98 [81] collaboration. Bass, Müller, Srivastava [6], have calculated two body quantum correlation of high energy photon using Parton Cascade Model (PCM) and ideal hydrodynamic model for central 200A GeV  $Au + Au$  collision at RHIC. They have shown that one can differentiate between the direct photons from early per-equilibrium stage and the same from later QGP and hadronic gas stages depending on features of the correlation function. Left panel of Fig. 31 shows that about 88% of the total photons having transverse momenta ( $1 \pm 0.1$ ) GeV (produced by hard parton scattering in PCM [82]) are emitted within a time period of 0.3 fm/c at rapidity  $y = 0$ . Right panel of the same figure shows that at  $k_T = 1$  GeV, the contribution of pre-equilibrium phase and thermal photons are similar to the total photon yield, whereas at  $k_T = 2$  GeV hard photons from PCM outshine the thermal ones by an order of magnitude. The emission time in PCM is very small and hydrodynamic calculation with  $\tau_0 = 0.3$  fm/c allows a smooth continuation of the emission rate. Intensity correlation for  $k_T \geq 2$  GeV (Fig. 31) reveals a pre-thermal photon dominated small size source of brief duration. On the contrary, for  $k_T = 1$  GeV we can see much larger radii for an extended source and suppression of pre-thermal contribution over thermal.

Intensity interferometry of thermal photons having transverse momentum  $k_T \sim 0.1 - 2.0$  GeV [43] provide an accurate information about the temporal and spatial structure of the interacting medium.

In reference [43] WA98 data is compared with theoretical results and prediction are given for RHIC and LHC energies. One dimensional correlation

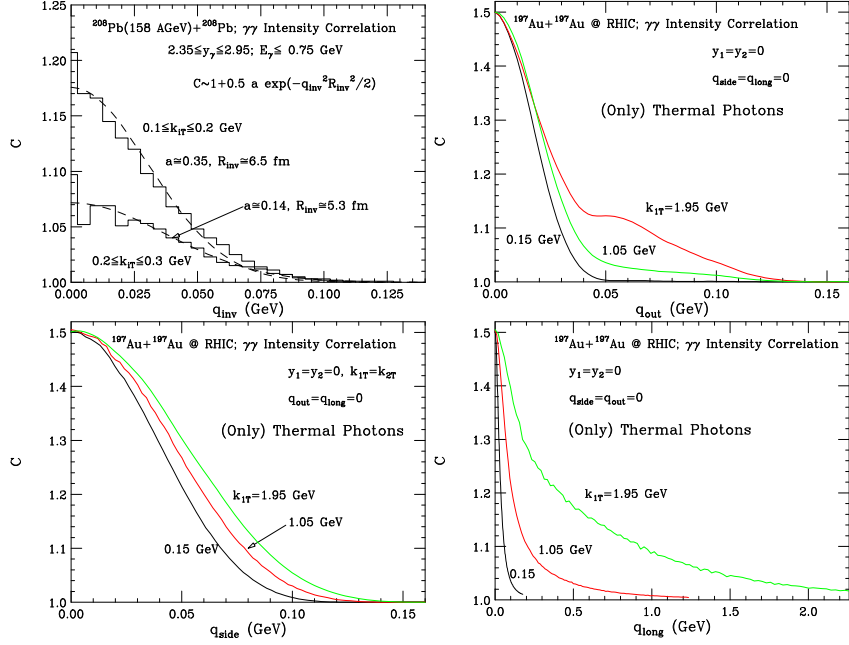


**Fig. 33.** One dimensional correlation function for the kinematic window used in WA98 experiment, assuming a fully source and emitting only single photon. Outward side-ward and longitudinal correlation function for thermal photons in central collision at RHIC energy. (taken from Ref. [43]).

function in terms of  $q_{inv}$  (invariant momentum difference) for different  $k_T$  and rapidity windows along with WA98 data is shown in figure 33. Theoretical results are well fitted in the form  $C = 1 + 0.5 a \exp[-q_{inv}^2 R_{inv}^2/2]$  and are in reasonable agreement with the experimental data. At RHIC energy, contribution from quark matter increases and as a result the two source aspect in the outward correlation radii become more clear. Similar results are obtained for LHC energies. It is found that the transverse momentum dependence of the different radii are quite different from the corresponding results for pions and do not decrease as  $1/\sqrt{m_T}$ . For SPS, RHIC, and LHC energies the longitudinal correlations show similar values, which can be explained as a result of boost invariance of the flow pattern.

## 8 Epilogue

We have tried to give a reasonably complete introduction to the exciting possibilities provided by radiation of direct photons and dileptons for the study of the dynamics of relativistic heavy ion collisions.

While low mass dileptons provide insights into the medium modification of vector mesons, those having intermediate masses carry signatures of thermal radiation from the quark gluon plasma. We have, due to lack of space, left out the discussion of correlated decay of charm and bottom mesons which give a large contribution to dileptons. These are also important as they carry valuable information about the extent of thermalization, elliptic flow, and energy-loss exhibited by heavy quarks.

We have discussed sources of direct photons, consisting of prompt photons, thermal radiation from quark and hadronic matter and those due to passage of jets through QGP. We have also seen that photons carry information about the initial temperature, evolution of elliptic flow, and size of the system. High statistics data at RHIC and LHC along with photon or dilepton tagged jets will go a long way in seeing that we realize the full potential of electromagnetic probes of quark gluon plasma.

## 9 Acknowledgment

This write up is based on the notes taken by RC and LB from the lectures given by DKS at the QGP Winter School 2008 at Jaipur. We thank the organizers for their warm hospitality. The work discussed here has benefited from discussions and collaborations with colleagues over many years and from many countries, and we take this opportunity to thank all of them and also to apologize to those whose work may not have found mention in these introductory lectures as this write up is not intended to be a review.

Finally we thank the organizers for their patience and for giving us extra time to complete this write up.

## References

1. B. Müller, *The Physics of Quark Gluon Plasma*, Springer, Heidelberg, 1985.
2. C. Y. Wong, *Introduction of High Energy Heavy Ion Collisions*, World Scientific, Singapore, 1994.
3. R. C. Hwa (ed.), *Quark Gluon Plasma*, Vol. I II, World Scientific, Singapore, 1990, 1995.
4. U. Heinz, CERN Yellow Report CERN-2004-001, arXiv: 0407360 [hep-ph].
5. E. L. Feinberg, *Nuovo Cim. A* **34**, 391 (1976).
6. S. A. Bass, B. Müller, and D. K. Srivastava, *Phys. Rev. Lett.* **93**, 162301 (2004); S. A. Bass, B. Müller, and D. K. Srivastava, *Phys. Rev. Lett.* **90**, 082301 (2003); *ibid.*, *Phys. Rev. C* **66**, 061902 (2002); T. Renk, S. A. Bass, and D. K. Srivastava, *Phys. Lett. B* **632**, 632 (2006).
7. R. Chatterjee, E. Frodermann, U. Heinz, and D. K. Srivastava, *Phys. Rev. Lett.* **96**, 202302 (2006); U. Heinz, R. Chatterjee, E. Frodermann, C. Gale, and D. K. Srivastava, *Nucl. Phys. A* **783**, 379 (2007).
8. R. Chatterjee and D. K. Srivastava, arXiv:0809.0548 [nucl-th].

9. R. J. Fries, B. Müller, and D. K. Srivastava, *Phys. Rev. Lett.* **90**, 132301 (2003).
10. K. Kajantie, J. Kapusta, L. McLerran, and A. Mekijan, *Phys. Rev. D* **34**, 2746 (1986).
11. M. M. Aggarwal *et al.* [WA98 Collaboration], *Phys. Rev. Lett.* **85**, 3595 (2000).
12. S. S. Adler *et al.* [PHENIX Collaboration], *Phys. Rev. Lett.* **94**, 232301 (2005).
13. S. S. Adler *et al.* [PHENIX Collaboration], *Phys. Rev. C* **76**, 034904 (2007).
14. A. Adare *et al.* [PHENIX Collaboration], arXiv: 0804.4168 [nucl-ex]; S. Bathe [PHENIX Collaboration], *Eur. Phys. J. C* **49**, 225 (2007).
15. N. M. Kroll and W. Wada, *Phys. Rev.* **98**, 1355 (1955).
16. L. G. Landsberg, *Phys. Rept.* **128**, 301 (1985).
17. H. Gong, [PHENIX Collaboration], Proceedings of 19th International Conference on Ultra-Relativistic Nucleus-Nucleus Collisions: Quark Matter 2006 (QM2006), Shanghai, China, 14-20 Nov 2006, arXiv:0705.1133 [nucl-ex]; T. Dahms *et al.*, *Eur. Phys. J. C* **49**, 249 (2007).
18. D. K. Srivastava, *J. Phys. G* **35**, 104026, 2008.
19. P. Aurenche, J.-P. Guillet, E. Pilon, and M. Werlen, *Phys. Rev. D* **73**, 094007 (2006).
20. P. Aurenche, M. Fontannaz, J.-P. Guillet, B. Kniehl, E. Pilon, and M. Werlen, *Eur. Phys. J. C* **9**, 107 (1999).
21. L. E. Gordon and W. Vogelsang, *Phys. Rev. D* **50**, 1901 (1994).
22. P. Aurenche, R. Basu, M. Fontannaz, and R. M. Godbole, *Eur. Phys. J. C* **42**, 43 (2005).
23. S. Jeon, J. Jalilian-Marian, and I. Sarcevic, *Nucl. Phys. A* **715**, 795 (2003); F. Arleo, *JHEP* **0609**, 015 (2006).
24. D. K. Srivastava [to be published].
25. T. Isobe [PHENIX Collaboration], *J. Phys. G* **34**, S1015 (2007).
26. L. D. McLerran and T. Toimela, *Phys. Rev. D* **31**, 545 (1985); H. A. Weldon, *Phys. Rev. D* **42**, 2384 (1990).
27. C. Gale and J. Kapusta, *Nucl. Phys. B* **357**, 65 (1991).
28. J. Kapusta, P. Lichard, and D. Seibert. *Phys. Rev. D* **44**, 2774 (1991), *Erratum-ibid* **47**, 4171 (1993).
29. R. Baier, H. Nakkagawa, A. Niegawa, and K. Redlich, *Z Phys. C* **53**, 433 (1992).
30. R. D. Pisarski, *Nucl. Phys. B* **309**, 476 (1988); *Phys. Rev. Lett.* **63**, 1129 (1989); E. Braaten and R. D. Pisarski, *Nucl. Phys. B* **337**, 569 (1990).
31. P. Arnold, G. D. Moore, and L. G. Yaffe, *JHEP* **0112**, 009 (2001).
32. H. Nadeau, *Phys. Rev. D* **48**, 3182 (1993).
33. S. Turbide, C. Gale, S. Jeon, and G. D. Moore, *Phys. Rev. C* **72**, 014906 (2005).
34. B. G. Zakharov, *JETP Lett.* **80**, 1 (2004).
35. S. Turbide, R. Rapp, and C. Gale, *Phys. Rev. C* **69**, 014903 (2004).
36. L. Xiong, E. V. Shuryak, and G. E. Brown, *Phys. Rev. D* **46**, 3798 (1992).
37. C. Song, *Phys. Rev. C* **47**, 2861 (1993).
38. J. Alam, P. Roy, and S. Sarkar, *Phys. Rev. C* **68**, 031901 (2003).
39. J. Alam, S. Sarkar, P. Roy, T. Hatsuda, and B. Sinha, *Ann. Phys.* **286**, 159 (2001).

40. R. Albrecht *et al.* [WA80 Collaboration], *Phys. Rev. Lett.* **76**, 3506 (1996).
41. D. K. Srivastava and B. Sinha, *Phys. Rev. Lett.* **73**, 2421 (1994).
42. J. Alam, D. K. Srivastava, B. Sinha, and D. N. Basu, *Phys. Rev. D* **48**, 1117 (1993).
43. D. K. Srivastava, *Phys. Rev. C* **71**, 034905 (2005).
44. R. C. Hwa and K. Kajantie, *Phys. Rev. D* **32**, 1109 (1985).
45. A. Dumitru, U. Katscher, J. A. Maruhn, H. Stöcker, W. Greiner, and D. H. Rischke, *Phys. Rev. C* **51**, 2166 (1995); N. Arbex, U. Ornik, M. Plümer, A. Timmermann, and R. M. Weiner, *Phys. Lett. B* **345**, 307 (1995); J. Sollfrank, P. Huovinen, M. Kataja, P. V. Ruuskanen, M. Prakash, and R. Venugopalan, *Phys. Rev. C* **55**, 392 (1997); J. V. Steele, H. Yamagishi, and I. Zahed, *Phys. Rev. D* **56**, 5605 (1997); T. Hirano, S. Muroya, and M. Namiki, *Prog. Theor. Phys.* **98**, 129 (1997); D. K. Srivastava and B. C. Sinha, *Eur. Phys. J. C* **12**, 109 (2000), *Erratum-ibid* **20**, 397 (2001).
46. J. Cleymans, K. Redlich, and D. K. Srivastava, *Phys. Rev. C* **55**, 1431 (1997).
47. D. K. Srivastava and B. Sinha, *Phys. Rev. C* **64**, 034902 (2001).
48. I. Kvasnikova, C. Gale, and D. K. Srivastava, *Phys. Rev. C* **65**, 064903 (2002).
49. J. Alam, S. Sarkar, T. Hatsuda, T. K. Nayak, and B. Sinha, *Phys. Rev. C* **63**, 021901 (2001).
50. P. Huovinen, P. V. Ruuskanen, and S. S. Rasanen, *Phys. Lett. B* **535**, 109 (2002); S. S. Rasanen, *Nucl. Phys. A* **715**, 717 (2003); H. Niemi, S. S. Rasanen, and P. V. Ruuskanen, CERN Yellow Report CERN-2004-009, arXiv:0311131 [hep-ph].
51. J. Alam, J. K. Nayak, P. Roy, A. K. Dutta-Mazumder, and B. Sinha, *J. Phys. G* **34**, 871 (2007).
52. D. G. d'Enterria and D. Peressounko, *Eur. Phys. J. C* **46**, 451(2006).
53. B. B. Back *et al.* [PHOBOS Collaboration], *Phys. Rev. C* **65**, 061901 (2002).
54. J. Kapusta, L. D. McLerran, and D. K. Srivastava, *Phys. Lett. B* **283**, 145 (1992).
55. R. J. Fries, B. Müller, and D. K. Srivastava, *Phys. Rev. C* **72** 041902(R) (2005).
56. S. Turbide, C. Gale, E. Frodermann, and U. Heinz, *Phys. Rev. C* **77**, 024909 (2008).
57. H. Busching [PHENIX Collaboration], *Nucl. Phys. A* **774**, 103 (2006).
58. K. Kajantie, M. Kataja, L. McLerran, and P. V. Ruuskanen, *Phys. Rev. D* **34**, 811 (1986).
59. G. Agakichiev *et al.* [CERES Collaboration] *Eur. Phys. J. C* **41**, 475 (2005).
60. D. Adamova *et al.* [CERES/NA45 Collaboration] *Phys. Rev. Lett.* **91**, 042301 (2003).
61. G. E. Brown and M. Rho, *Phys. Rept.* **269**, 333 (1996).
62. R. Rapp and J. Wambach, *Eur. Phys. J. A* **6**, 415 (1999).
63. M. Masera *et al.*, *Nucl. Phys. A* **590**, 93c (1995); A. L. S. Angelis *et al.*, *Eur. Phys. J. C* **13**, 433 (2000).
64. M. C. Abreu *et al.* [NA38/NA50 Collaboration], *Eur. Phys. J. C* **14**, 443 (2000).
65. R. Rapp and E. V. Shuryak, *Phys. Lett. B* **473**, 13 (2000).
66. R. Arnaldi *et al.* [NA60 Collaboration], *Phys. Rev. Lett.* **96**, 162302 (2006).
67. H. van Hees and R. Rapp, *Phys. Rev. Lett.* **97**, 102301 (2006).
68. J. -Y. Ollitrault, *Phys. Rev. D* **46**, 229 (1992).

69. U. W. Heinz and A. Kuhlman, *Phys. Rev. Lett.* **94**, 132301 (2005).
70. P. F. Kolb and U. Heinz, *Quark-Gluon Plasma 3*, edited by R. C. Hwa and X.-N. Wang (World Scientific, Singapore, 2004) arXiv: 0305084 [nucl-th].
71. R. Chatterjee, D. K. Srivastava, and U. Heinz, Proceedings of 20th International Conference on Ultra-Relativistic Nucleus-Nucleus Collisions: Quark Matter 2008 (QM2008), Jaipur, India, 4-10 Feb. 2008; R. Chatterjee, D. K. Srivastava, and U. Heinz, Proceedings of International Conference on Particle and Nuclei (PANIC08), Eilat, Israel, 9-14 Nov, 2008, arXiv: 0901.3270 [nucl-th].
72. R. Chatterjee, D. K. Srivastava, U. Heinz, and C. Gale, *Phys. Rev. C* **75**, 054909 (2007).
73. R. N. Cahn, *Phys. Rev. D* **7**, 247 (1973); C. Gale and J. Kapusta, University of Minnesota Report No. 88/2, 1988 (unpublished).
74. B. Layek, R. Chatterjee, and D. K. Srivastava, *Phys. Rev. C* **74**, 044901 (2006).
75. T. Sakaguchi [PHENIX Collaboration], arXiv: 0705.1711 [nucl-ex].
76. Kentaro Miki, Proceedings of 19th International Conference on Ultra-Relativistic Nucleus-Nucleus Collisions: Quark Matter 2006 (QM2006), Shanghai, China, 14-20 Nov 2006, Shanghai, China, November 2006.
77. X.-N. Wang, Z. Huang, and I. Sarcevic, *Phys. Rev. Lett.* **77**, 231 (1996).
78. T. Renk, *Phys. Rev. C* **74**, 034906 (2006).
79. D. K. Srivastava, C. Gale, and T. C. Awes, *Phys. Rev. C* **67**, 054904 (2003).
80. I. P. Lokhtin, A. V. Sherstnev, and A. M. Snigirev, *Phys. Lett. B* **599**, 260 (2004).
81. M. M. Aggarwal *et al.* [WA98 Collaboration], *Phys. Rev. Lett.* **93**, 022301 (2004).
82. S. Turbide, C. Gale, and R. J. Fries, *Phys. Rev. Lett.* **96**, 032303 (2006).